AGU PUBLICATIONS

Tectonics

RESEARCH ARTICLE
10.1002/2014TC003706

Key Points:
- Northern PCSS deformed at circa 2.48 Ga during dextral strike-slip motion
- Southern PCSS deformed at circa 740–550 Ma during dextral transpression
- Madurai Block deformation constrained to circa 550–500 Ma

Supporting Information:
- Appendix S1

Correspondence to:
D. Plavsa,
diana.plavsa@curtin.edu.au

Citation:
Plavsa, D., A. S. Collins, J. D. Foden, and C. Clark (2015), The evolution of a Gondwanan collisional orogen: A structural and geochronological appraisal from the Southern Granulite Terrane, South India, *Tectonics*, *34*, 820–857, doi:10.1002/2014TC003706.

Received 18 AUG 2014
Accepted 28 MAR 2015
Accepted article online 22 APR 2015
Published online 6 MAY 2015

The evolution of a Gondwanan collisional orogen: A structural and geochronological appraisal from the Southern Granulite Terrane, South India

Diana Plavsa[1,2], Alan S. Collins[1], John D. Foden[1], and Chris Clark[2]

[1]Centre for Tectonics, Resources and Exploration, Department of Earth Sciences, University of Adelaide, Adelaide, South Australia, Australia, [2]The Institute for Geoscience Research, Department of Applied Geology, Curtin University of Technology, Perth, Western Australia, Australia

Abstract Gondwana amalgamated along a suite of Himalayan-scale collisional orogens, the roots of which lace the continents of Africa, South America, and Antarctica. The Southern Granulite Terrane of India is a generally well-exposed, exhumed, Gondwana-forming orogen that preserves a record of the tectonic evolution of the eastern margin of the East African Orogen during the Ediacaran-Cambrian (circa 600–500 Ma) as central Gondwana formed. The deformation associated with the closure of the Mozambique Ocean and collision of the Indian and East African/Madagascan cratonic domains is believed to have taken place along the southern margin of the Salem Block (the Palghat-Cauvery Shear System, PCSS) in the Southern Granulite Terrane. Investigation of the structural fabrics and the geochronology of the high-grade shear zones within the PCSS system shows that the Moyar-Salem-Attur shear zone to the north of the PCSS system is early Paleoproterozoic in age and associated with dextral strike-slip motion, while the Cauvery shear zone (CSZ) to the south of the PCSS system can be loosely constrained to circa 740–550 Ma and is associated with dip-slip dextral transpression and north side-up motion. To the south of the proposed suture zone (the Cauvery shear zone), the structural fabrics of the Northern Madurai Block suggest four deformational events (D_1–D_4), some of which are likely to be contemporaneous. The timing of high pressure-ultrahigh temperature metamorphism and deformation (D_1–D_3) in the Madurai Block (here interpreted as the southern extension of Azania) is constrained to circa 550–500 Ma and interpreted as representing collisional orogeny and subsequent orogenic collapse of the eastern margin of the East African Orogen. The disparity in the nature of the structural fabrics and the timing of the deformation in the Salem and the Madurai Blocks suggest that the two experienced distinct tectonothermal events prior to their amalgamation along the Cauvery shear zone during the Ediacaran/Cambrian.

1. Introduction

The circa 650–500 Ma assembly of the continental domains that made up the supercontinent Gondwana took place along a number of dispersed Proterozoic mobile belts [*Meert and Van Der Voo*, 1997; *Stern*, 2002; *Meert*, 2003; *Collins and Pisarevsky*, 2005]. Of those, the Himalayan-scale East African Orogen (EAO) extending from northeast Africa, through western Arabia, East Africa, Madagascar, South India, Sri Lanka, and Antarctica [*Kriegsman*, 1995; *Boger and Miller*, 2004; *Jacobs and Thomas*, 2004; *Collins and Pisarevsky*, 2005; *Prakash et al*., 2006; *Fritz et al*., 2013], marks a belt of highly deformed and metamorphosed Precambrian rocks that were reworked during the final stages of Gondwana amalgamation. The tectonic style of the EAO orogen changes from predominantly juvenile accretionary tectonics of the Arabian-Nubian Shield at the northern margin [*Johnson et al*., 2011; *Robinson et al*., 2014] to continental-style collisional tectonics toward the south [*Meert and Van Der Voo*, 1997; *Collins and Pisarevsky*, 2005; *Prakash et al*., 2006; *Fritz et al*., 2013]. The timing of the metamorphism associated with the collisional-style tectonics differs across the orogen from west to east. Along the western margin of the EAO (through East Africa), the timing of the high-pressure granulite-facies metamorphism and reworking of Precambrian terranes are constrained to between circa 650 and 620 Ma [*Muhongo and Lenoir*, 1994; *Appel et al*., 1998; *Reddy et al*., 2004; *Sommer et al*., 2005; *Jöns and Schenk*, 2011]. In contrast, the eastern margin of the EAO marks the site of Mozambique Ocean closure during the Malagasy Orogeny [*Meert and Van der Voo*, 1997; *Collins and Windley*, 2002; *Collins*

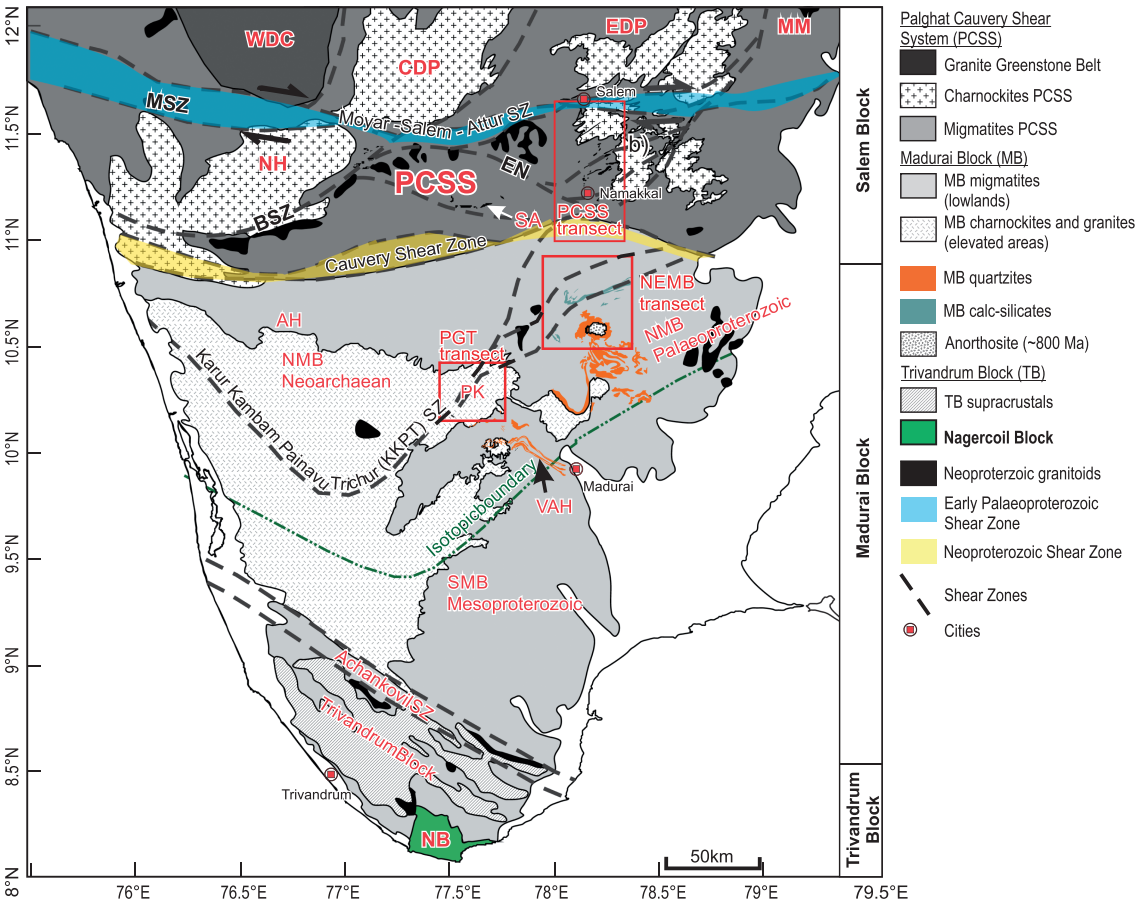

Figure 1. Regional geological map of the Southern Granulite Terrane and the location of the mapped transects. WDC, Western Dharwar Craton; CDP, Central Dharwar Province; EDP, Eastern Dharwar Province; MM, Madras massifs; MSZ, Moyar shear zone; NH, Nilgiri Hills; BSZ, Bhavani shear zone; EN, Erode-Namakkal shear zone; SA, Sittampundi Anorthosite Complex; AH, Anaimalai Hills; NMB, Northern Madurai Block; KP, Kodaikanal-Palni Hills; VAH, Varushanad-Andipatti Hills; NB, Nagercoil Block.

and Pisarevsky, 2005; *Cawood and Buchan*, 2007] across a number of suture zones including (1) the Betsimisarka Suture in Madagascar [*Collins et al*., 2001; *Collins and Windley*, 2002; *Collins et al*., 2003] and (2) the Cauvery shear zone (CSZ) in Southern India [*Collins et al*., 2007a; *Clark et al*., 2009a; *Santosh et al*., 2009; *Sato et al*., 2011a] and quite possibly Lützow-Holm bay in Antarctica [*Fraser et al*., 2000; *Collins and Pisarevsky*, 2005; *Tsunogae et al*., 2014]. The timing of the Malagasy Orogeny has been constrained to 550–510 Ma [*Meert*, 2003; *Collins*, 2006; *Collins et al*., 2007a; *Clark et al*., 2009a; *Jöns and Schenk*, 2011; *Collins et al*., 2014a].

In Southern India, the Malagasy Orogeny is characterized by intense reworking of Precambrian lithologies at the southern margin of the Palghat-Cauvery Shear System (PCSS), and pervasive metamorphism and deformation throughout the Madurai, Trivandrum, and Nagercoil Blocks (Figure 1) [*Cenki et al*., 2004; *Ghosh et al*., 2004; *Chetty and Bhaskar Rao*, 2006a; *Collins et al*., 2007a; *Clark et al*., 2009a; *Plavsa et al*., 2012; *Collins et al*., 2014a; *Plavsa et al*., 2014; *Johnson et al*., 2015; *Clark et al*., 2009a, 2014]. It is believed that the Cauvery shear zone (CSZ, southernmost shear zone in the PCSS system) brings together the deformed and metamorphosed southern margin of the Indian Dharwar Craton to the north (the Salem Block) and the northern margin of the proposed microcontinent Azania [*Collins and Windley*, 2002; *Collins and Pisarevsky*, 2005], here termed the Madurai Block. Limited, structurally constrained, geochronological studies have provided some insight into the kinematic evolution of the Cauvery shear zone [*Meißner et al*., 2002; *Ghosh et al*., 2004], while others were focused on the structural interpretations based on satellite imagery combined with field work observations [*Drury and Holt*, 1980; *Drury et al*., 1984; *Chetty and Bhaskar Rao*, 2006b; *Chetty and Bhaskar Rao*, 2006c]. The distinct polydeformational histories of the Precambrian terranes involved in the Ediacaran-Cambrian Malagasy Orogeny have led to ambiguities with the interpretation of the timing of individual structural fabrics, particularly in the zones of intense deformation

and partial melting of the exposed lower crustal domains. In recent times, the Palghat-Cauvery Shear System (PCSS) has been variously described as a dextral transpressive orogen with a "flower structure" at its southern margin, a collapsed marginal basin, and a cryptic suture zone [*Drury and Holt*, 1980; *Drury et al*., 1984; *Chetty and Bhaskar Rao*, 2006b; *Chetty and Bhaskar Rao*, 2006c; *Collins et al*., 2007a]. The dextral transpression model is in marked contrast to the proposed sinistral transpressional system invoked by *Jacobs and Thomas* [2004] for the evolution of the East African Orogen and the lateral escape tectonics model. In addition, the interpretation of the Cauvery shear zone as a late Neoproterozoic suture zone in the Southern Granulite Terrane of India has recently been contested by a number of authors [*Bhaskar Rao et al*., 2003; *Ghosh et al*., 2004; *Brandt et al*., 2011; *Tucker et al*., 2011a, 2011b; *Brandt et al*., 2014]. These studies favor the model whereby the Indian crust (the Dharwar Craton) extends to the south of the Cauvery shear zone, down to the Karur-Kambam-Painavu-Trichur (KKPT) shear zone (Figure 1). Most recently, *Brandt et al*. [2014] suggested that the Southern Granulite Terrane of India represents the extension of the Paleoproterozoic to Mesoproterozoic Ongole Domain (Eastern Ghats) that straddles the eastern margin of peninsular India. Such reconstructions invoke km scale (between 150 and 200 km) dextral strike-slip offsets along the Cauvery shear zone.

In this paper, we appraise the structural and temporal evolution of both the proposed suture zone and the individual crustal blocks (Salem Block and Madurai Block) brought together by this suture in the late Neoproterozoic to test the various hypotheses of the formation and evolution of this central part of the Gondwana-forming orogen network.

2. Regional Geochronological and Structural Framework for the Southern Granulite Terrane

The Southern Granulite Terrane of India is located at the southern tip of the Indian subcontinent and in the broader tectonic context belongs to the Proterozoic mobile belt at the southern margin of the greater Archean Dharwar Craton [*Drury and Holt*, 1980; *Drury et al*., 1984; *Tucker et al*., 2011a; *Tucker et al*., 2011b]. This is sometimes known as the Pandyan Mobile Belt [*Ramakrishnan*, 1993]. The transition from predominantly greenschist- to amphibolite-facies rocks of the Dharwar Craton to the lower crustal exposures of the Southern Granulite Terrane is gradual and is represented by dehydration and deformation of the amphibolite-facies tonalite-trondjemite-granite gneisses to orthopyroxene-bearing felsic gneisses (charnockites) without any lithological or structural breaks [*Pichamuthu*, 1960; *Janardhan et al*., 1979; *Drury et al*., 1984; *Santosh et al*., 1990; *Hansen and Harlov*, 2007]. The Southern Granulite Terrane is divided into a number of distinct crustal blocks based on the structural and isotopic evolution, and they include the following, from north to south: (1) the Salem Block, (2) the Madurai Block, (3) the Trivandrum Block, and (4) the Nagercoil Block [*Bartlett et al*., 1998; *Santosh*, 1996; *Clark et al*., 2009b; *Santosh et al*., 2009; *Plavsa et al*., 2012; *Collins et al*., 2014a]. The summary of the main thermo-tectonic events within the Southern Granulite Terrane is given in Table 1 with a comprehensive review given by *Collins et al*. [2014a].

To date, a number of regional-scale structural studies concerning peninsular India have been carried out using satellite imagery combined with limited field observations as the primary tools. Of those, the studies by *Drury and Holt* [1980] and *Drury et al*. [1984] were among the first to describe the crustal-scale structural framework of the Southern Granulite Terrane of India. They considered the N-S trending structural fabrics of the Dharwar Craton to have been reworked by E-W trending crustal-scale shear zones (Palghat-Cauvery Shear System) sometime after the Neoarchean. They correlated the shearing along the Moyar-Salem-Attur shear zone at the northernmost margin of the Palghat-Cauvery Shear System with the development of a middle to late Proterozoic fold and thrust belt along the eastern margin of the Cuddapah Basin in the Neoarchean Eastern Dharwar Craton farther north [*Drury and Holt*, 1980, and references therein]; this eastern Cuddapah Basin fold and thrust belt form the Nallamala Hills and have recently been shown to be Mesoprotoerozoic-Neoproterozoic in age [*Collins et al*., 2014b]. U-Pb geochronological studies of zircons and monazites from within the Palghat-Cauvery Shear System suggest that the Neoarchean (circa 2.7–2.5 Ga) basement protoliths were affected by granulite-facies metamorphism during the early Paleoproterozoic (circa 2.5–2.48 Ga) [*Raith et al*., 1999; *Ghosh et al*., 2004; *Anderson et al*., 2012; *Brandt et al*., 2014; *Mohan et al*., 2013; *Glorie et al*., 2014]. They were subsequently

Table 1. Summary of Main Tectonic Events in the Southern Granulite Terrane

Salem Block	2.9–2.5 Ga basement crystallization ages (U-Pb zircon)
	3.4–2.4 Ga basement whole rock Nd model ages
	2. 5–2.45 Ga high-P granulite-facies metamorphism (northern Salem Block in the vicinity of Moyar-Attur shear zone), the extent of this metamorphic event toward the Palghat-Cauvery shear zone is uncertain.
	735–720 Ma poorly defined thermal event (Sm-Nd garnet-plagioclase-hornblende-WR isochron age, U-Pb zircon age)
	535–525 Ma late Neoproterozoic high P-T (>12 kbar, >950°C) metamorphic event common at the southern margin of the Salem Block (in the vicinity of Palghat-Cauvery shear zone)—Collisional tectonics associated with Gondwana amalgamation
Northern Madurai Block (NMB)	2.5 Ga basement ages north western part of the Madurai Block (NWMB—north of KKPT shear zone)
	820–750 Ma granites, tonalites, and gabbros intruding into 2.5 Ga basement and supracrustal rocks
	3.4–1.7 Ga detrital zircon spectra of supracrustal units in the north eastern part of the Madurai Block (NEMB), NE of the KKPT shear zone
	3.0–2.4 Ga whole rock Nd model ages of orthogneisses and paragneisses throughout Northern Madurai Block (NMB)
	550–530 Ma high-grade HP-UHT metamorphism (7–11 kbar, 950–1150°C)
Southern Madurai Block (SMB)	1000–790 Ma magmatic crystallization ages
	1.6–1.2 Ga whole rock Nd model ages of the orthogneisses and paragneisses
	1100–650 Ma detrital zircon spectra of the supracrustal units
	550–520 Ma HP-UHT metamorphism (7–11 kbar, 950–1150°C)
Achankovil shear zone	1500–950 Ma magmatism U-Pb zircon age
	2000–650 Ma detrital zircon age range
	2.0–1.2 Ga whole rock Nd model ages of orthogneisses and paragneisses
	600–500 Ma HP-UHT metamorphism (8–10 kbar, 940–1040°C) and syntectonic to posttectonic A-type magmatism
Trivandrum Block (TB)—including Nagercoil Block	2.0–1.8 Ga and 950 Ma magmatic crystallization U-Pb zircon age
	3.0–1.7 Ga detrital zircon spectra of supracrustal units (Kerala Khondalite Belt)
	2.5–2.0 Ga whole rock Nd model ages of orthogneisses and paragneisses
	550–500 Ma HP-HT metamorphism (8–9 kbar, <1000°C)

retrogressed along localized shear zones associated with metamorphic fluid-channeling to amphibolite-facies, biotite-bearing gneisses. The timing of this retrogressive event has been loosely constrained to between circa 730 and 500 Ma based on Sm-Nd garnet whole rock and Rb-Sr biotite dating of retrogressed granulites and posttectonic pegmatites [*Bhaskar Rao et al*., 1996; *Meißner et al*., 2002; *Mohan et al*., 2013]. *Drury et al*. [1984] acknowledged the marked change in lithology and structural character of the Madurai and Trivandrum Blocks south of the Palghat-Cauvery Shear System, but the lack of geochronological data hindered further interpretation. Nonetheless, they described the supracrustal-dominated Madurai and Trivandrum Blocks as marginal shelf sequences deposited on the basement rocks of the Northern Madurai Block (the Kodaikanal-Palni Hills, Figure 1) subsequently deformed during a crustal-thickening event associated with continent-continent collisional orogeny [*Drury et al*., 1984].

Subsequent work by *Ghosh et al*. [2004] and *Cenki and Kriegsman* [2005] focused on the tectonic evolution of the Southern Granulite Terrane in particular. *Ghosh et al*. [2004] combined field and structural observations with isotope dilution-thermal ionization mass spectrometry (TIMS), sensitive high-resolution ion microprobe (SHRIMP), and zircon evaporation U-Pb geochronology to better constrain the deformational events. They carried out six traverses across the major shear zones [*Ghosh et al*., 2004, Figure 1] and suggested that seven major tectonothermal events took place in the Southern Granulite Terrane at circa 2.5 Ga, circa 2.0 Ga, circa 1.6 Ga, circa 1.0 Ga, circa 800 Ma, circa 600 Ma, and circa 550 Ma. The conclusions of the study completed by *Ghosh et al*. [2004] include extension of the Archean (circa 2.7–2.5 Ga) Dharwar Craton crust south of the Cauvery shear zone to the Karur-Kambam-Painavu-Trichur shear zone (KKPT, Figure 1), where the basement protoliths yielded Neoarchean to Early Paleoproterozoic crystallization ages (circa 2.65–2.43 Ga) [*Bartlett et al*., 1998; *Brandt et al*., 2011; *Plavsa et al*., 2012; *Bhattacharya et al*., 2014; *Brandt et al*., 2014]. They interpreted the KKPT shear zone as either a major terrane boundary or a tectonized décollement between the basement rocks to the north and the supracrustal assemblages to the east and south. The timing of the deformation along the major shear zones in the Southern Granulite

Terrane was suggested to occur as an early Neoproterozoic phase (circa 800–700 Ma, D_2) and a late Neoproterozoic phase between 550 and 530 Ma (D_3), followed by rapid uplift and retrogression between 525 and 480 Ma [*Ghosh et al*., 2004]. The earlier deformation within the Palghat-Cauvery Shear System (D_1), particularly at the northern margins near the Moyar-Salem-Attur shear zone, was attributed to the development of gneissic fabrics during high-pressure metamorphism at circa 2.5–2.45 Ga [*Raith et al*., 1999; *Ghosh et al*., 2004].

The study by *Cenki and Kriegsman* [2005] was focused on the tectonic evolution of the Madurai and Trivandrum Blocks south of the Cauvery shear zone. Their study identified three major deformational events, with the early development of the gneissic fabrics (D_1) assigned to the high-grade late Neoproterozoic (circa 580–550 Ma) metamorphism and the subsequent D_2–D_3 fabrics to partial exhumation of the terrane. *Cenki and Kriegsman* [2005] suggested that the second deformational phase (D_{2a} and D_{2b}) was a product of a single continuous event and attributed the difference in structural character (NE-SW trending fabrics in the east, to NW-SE trending fabrics in the west) to a regionally variable stress field created around an "indenter" located offshore, to the SE of the Madurai Block. Furthermore, development of the subsequent E trending and ESE trending shear zones (D_3, Cauvery and Achankovil shear zones, respectively) was considered to be coeval and attributed to pure shear flattening during NNW-SSE shortening under retrograde conditions [*Cenki and Kriegsman*, 2005]. In their paper, *Cenki and Kriegsman* [2005] disagreed with *Ghosh et al*.'s [2004] interpretation of the KKPT shear zone being a major terrane boundary.

A closer scrutiny of the KKPT shear zone through remote sensing techniques and field observations was carried out by *Srinivasan and Rajeshdurai* [2010] who refer to the eastern segment of the KKPT shear zone as the Suruli shear zone. The structural character of the Suruli shear zone is defined by an easterly dipping mylonitic fabric that changes orientation from predominantly NE trending in the south to ENE trending as it heads north. They suggest that the continuously E dipping fabrics of the Suruli shear zone separate the massif-dominated western terrane (footwall) from the low-lying supracrustal sequences of the eastern terrane (hanging wall). This observation contrasts with that of *Drury et al*. [1984], who suggested that the supracrustal rocks of the eastern Madurai Block underlie the charnockite massifs to the west. To determine the kinematics of the Suruli shear zone, *Srinivasan and Rajeshdurai* [2010] identified three distinct folding phases (F_1 to F_3) in the eastern "hanging wall" block and only a single folding phase in the western "footwall" block, which they interpreted as coeval with F_3 folding in the eastern hanging wall block. This observation led them to suggest that the eastern block is older and thrust over the relatively younger western block in a top to the NW movement. However, subsequent U-Pb zircon geochronology and Sm-Nd whole rock isotopic analyses of the basement and cover rocks in Madurai Block [*Teale et al*., 2011; *Plavsa et al*., 2012; *Tomson et al*., 2013; *Brandt et al*., 2014; *Plavsa et al*., 2014] refute this interpretation.

To characterize the nature of the Palghat-Cauvery Shear System (PCSS), *Chetty and Bhaskar Rao* [2006a, 2006b] carried out comprehensive field studies combined with remote sensing and large-scale mapping. They identified two separate deformational events, with the early development of gneissic fabrics that were subsequently transposed by heterogeneously distributed strain characterized by high-strain E-W trending shear zones (the Moyar-Salem-Attur shear zone and the Cauvery shear zone) with shallow to moderate east plunging lineations and lower strain, fold-dominated domains (F_2). In addition, *Chetty and Bhaskar Rao* [2006a, 2006b] suggest that the fold-dominated, lower strain domains are transposed by NE trending sigmoidal shear zones connecting the Moyar-Salem-Attur shear zone and the Cauvery shear zone and, as a result, modeled the Palghat-Cauvery Shear System as a crustal-scale flower structure that formed during dextral transpression.

The plethora of contrasting structural observations and interpretations regarding the structural evolution of the Southern Granulite Terrane is a direct consequence of limited field observations, lack of structurally constrained geochronological data, and limitations of remote sensing methods due to extensive cover in certain parts of the orogen. This paper aims to address some of the above-mentioned issues by combining the U-Pb zircon geochronology of structurally constrained fabrics and crosscutting pegmatites with field observations and satellite imagery methods. This paper aims to provide better constraints on the tectonic evolution of the Palghat-Cauvery Shear System as well as the nature of the basement/cover relationship at the north eastern extension of the KKPT shear zone in the Northern Madurai Block.

3. Analytical Methods

Seven samples were selected from across the Palghat-Cauvery Shear System and the Northern Madurai Block for zircon U-Pb dating in order to constrain the timing of deformation and metamorphism. The summary of the results of the U-Pb dating are listed in Table 2, and the full data set is given in the Appendix A. Samples were crushed and sieved to obtain the 79–400 μm fraction. The sieved fraction was panned after which the zircon fraction was extracted using methylene iodide heavy liquids. The magnetic minerals were extracted using the hand magnet and zircons handpicked and mounted in epoxy resin disks. The polished mounts were carbon coated and zircons imaged under cathodoluminescence (CL) on a Philips XL40 scanning electron microscope (SEM) operating in high-vacuum mode with a tungsten filament with attached Gatan CL at Adelaide Microscopy (University of Adelaide).

Zircon grains were analyzed on a New Wave 213 nm Nd-YAG laser coupled with the Agilent 7500cs Inductively Coupled Plasma Mass Spectrometer (ICP-MS) at Adelaide Microscopy (University of Adelaide). Laser specifications and methods used are given in *Plavsa et al.* [2012]. The GEMOC GJ-1 standard zircon was used with published thermal ionization mass spectrometry (TIMS) normalizing ages of $^{207}Pb/^{206}Pb = 607.7 \pm 4.3$ Ma, $^{206}Pb/^{238}U = 600.7 \pm 1.1$ Ma, and $^{207}Pb/^{235}U = 602.0 \pm 1.0$ Ma [*Jackson et al.*, 2004] to correct for downhole fractionation and instrumental drift. Over the course of the analysis sessions, a total of 106 analyses of the GJ-1 external standard yielded a weighted average $^{207}Pb/^{206}Pb$ age of 609.2 ± 6.4 Ma (2σ, MSWD = 0.39) and $^{206}Pb/^{238}U = 600.6 \pm 1.6$ Ma (2σ, MSWD = 0.36). The Plešovice zircon standard (TIMS $^{206}Pb/^{238}U$ age = 337.13 ± 0.37 Ma, 95% confidence limits) [*Sláma et al.*, 2008] was used to check for accuracy during the analysis of unknowns. A total of 36 analyses of the Plešovice internal standard yielded a weighted average age of $^{206}Pb/^{238}U = 338.0 \pm 1.6$ Ma (2σ, MSWD = 1.2) demonstrating the accuracy of the operating conditions.

4. Structure and Geochronology of the Southern Granulite Terrane

The new data presented here consist of three traverses (Figure 1), from north to south they include (1) the Palghat-Cauvery Shear System traverse (north of the Cauvery shear zone), (2) the NE Madurai Block traverse (immediately south of the Cauvery shear zone), and (3) the Palni-Ganguvarpatti traverse (PGT) within the Northern Madurai Block. The primary objective is to determine the structural character of the proposed late Neoproterozoic suture zone (Palghat-Cauvery Shear System and the NE Madurai Block transects) and to determine the nature of the contact between the Archean charnockite massifs (elevated areas) west of the KKPT shear zone and the low-lying supracrustal units toward the east (Palni-Ganguvarpatti transect).

4.1. PCSS

The Palghat-Cauvery Shear System traverse extends approximately 75 km in N-S direction from the Moyar-Salem-Attur shear zone in the north to the Cauvery shear zone in the south (Figure 1). The main lithologies comprise granitic and tonalitic gneisses with dismembered garnet-bearing mafic granulites and ultramafic rocks, magnetite-rich quartzites and charnockites. Overall, the structural fabric of the Palghat-Cauvery Shear System transect includes folded low-strain gneiss domains bound by steeply to moderately dipping planar high-strain zones that coalesce to form a sigmoidal pattern with recognition of seven separate structural fabrics from north to the south of the PCSS transect. The Palghat-Cauvery Shear System is separated into four distinct domains based on different structural and geometric style. However, only minor changes in the proportion of certain lithologies can be recognized between each domain. The different deformational events in the PCSS transect are termed DP_1 to DP_5 with the corresponding structural fabrics SP_1 to SP_5. Letter subscripts indicate structural fabrics associated with loosely constrained deformational events. For example, DP_{3a} and DP_{3b} are believed to have occurred between 740 and 550 Ma where DP_{3a} predates DP_{3b}, but the exact timing for each remains unknown.

4.1.1. Domain 1

Domain 1 corresponds to a ~4 km wide zone crossing the Moyar-Salem-Attur shear zone in the northernmost part of the transect (Figure 2) and preserves two of the earliest fabrics (SP_1 and SP_2). The area that was mapped includes a well-known locality, the Kanja Malai Hills (Figure 2), an E-W trending elliptical shaped hillock characterized by high-strain ~E-W trending planar fabrics. The lithological units observed in this

Table 2. LA-ICP-MS U-Pb Zircon Age Dating of Structurally Constrained Lithologies From Across the PCSS and NMB[a]

Sample Description	Structural Evolution	Zircon Morphology and Texture Under CL	Age Interpretation and Geological Significance
		PCSS transect—Domain 2	
SI10-24—Bt-bearing granodioritic gneiss 11°24′21.1″N 78°13′52.9″E	Well foliated. Foliation defined by preferential orientation of biotite. Contains pyroxenite (opx-cpx) enclaves. NE-SW trending foliation parallel to the axial planes of the regional FP_2 folds	Zircons in this sample are round and range in size from 100 to 500 μm. The aspect ratios are typically 2:1. The internal zonation reveals highly recrystallized nature of the zircons typical of zircons associated high-grade metamorphism. Following textural domains were observed: 1. Oscillatory-zoned cores (Figure 5a, grains I and III) 2. Bright to moderately luminescent zircons with faint irregular or sector-zoned patterns (Figure 5a, grain II) 3. Sector-zoned inner rims surrounding the oscillatory-zoned cores (Figure 5a, grain III) 4. Ghost-zoned rims 5. Bright luminescent featureless rims	Oscillatory-zoned cores have yielded a weighted average $^{207}Pb/^{206}Pb$ age of 2534 ± 17 Ma (n = 6, 2σ, MSWD = 1.17) here interpreted as the crystallization age of the protolith. Bright luminescent outer and sector-zoned inner rims, ghost-zoned rims, and bright luminescent sector-zoned zircon grains are here interpreted as recrystallization of protolith zircon and growth of new zircon during metamorphism [*Corfu et al.*, 2003]. They yielded a combined weighted average $^{207}Pb/^{206}Pb$ age of 2501 ± 13 Ma (n = 15, 2σ, MSWD = 1.6), here interpreted as the age of metamorphism that resulted in development of the S_2 fabric in the granodiorite.
		PCSS transect—Domain 3	
SI10-62—Pegmatite 11°20′41.2″N 78°10′16.6″E	The pegmatite is undeformed and intrudes along sheared north dipping lower limbs of mesoscale recumbent folds (FP_4, Figures 7a and 7b). The country rock is retrogressed to bt-hbl-bearing assemblages along the shear zones and around the pegmatites	Zircon grains in this sample were scarce and significantly damaged due to radiation resulting from high concentrations of U and Th. Zircon grains are quite euhedral with aspect ratios of up to 4:1 and up to 600–700 μm long. Under CL, all zircons had similar textures which include the following: 1. Dark luminescent, highly metamict cores with occasional oscillatory-zoned domains (Figure 5b, grains I and II). During analysis, only oscillatory zoned domains were analyzed when observed. Analyses with high common Pb were discarded.	Dark oscillatory-zoned cores yielded a weighted average $^{206}Pb/^{238}U$ age of 554 ± 9 Ma (n = 3, 2σ, MSWD = 1.5)
		PCSS transect—Domain 4	
SI10-53—Kfs-qtz-bt-rich crosscutting leucosome 11°07′27.5″N 78°09′11.8″E	This sample is located immediately south of the Cauvery Shear Zone shear zone and comes from a late melt cutting across hbl-bt-migmatite that is well foliated. In places, layer-parallel leucosomes appear to be feeding the late crosscutting melt (Figure 7c) and could, therefore, be contemporaneous.	Zircon grains in this sample are euhedral to subhedral. They are up to 700 μm and have aspects ratios of up to 4:1. The internal textural zonation was consistent across majority of the zircons and includes the following: 1. Featureless moderately luminescent cores with irregular abraded margins surrounded by a thin bright luminescent band (inherited cores, Figure 5c, grain III)	Type 1 zircon grains yielded early Paleoproterozoic to Neoarchean ages (one concordant grain of 2442 ± 26 Ma, Figure 5c, grain III) Type 2 zircon textures are here interpreted as recrystallization of protolith zircon during migmatization and are here grouped together with type 3 zircon textures (oscillatory- to sector-zoned overgrowths, growth from melt) to yield a combined weighted average $^{206}Pb/^{238}U$ age of 556 ± 14 Ma (n = 8, 2σ, MSWD = 4.2).

Table 2. (continued)

Sample Description	Structural Evolution	Zircon Morphology and Texture Under CL	Age Interpretation and Geological Significance
		2. Completely recrystallized cores defined by bulbous bright luminescent patches overprinting what appear to be dark luminescent metamict cores (Figure 5c, grains I and IV)	This age is within error of the weighted average $^{207}Pb/^{206}Pb$ age of 563 ± 31 Ma (n = 8, 2σ, MSWD = 0.13) but has much lower MSWD thus validating the late Neoproterozoic age of metamorphism and migmatization. Low Th/U ratio (<0.1, Figure 6c) attests to the metamorphic nature of the analyzed zircon grains [*Hoskin and Black,* 2000].
		3. Oscillatory- to sector-zoned whole zircons or overgrowths mantling the inherited cores (Figure 5c, grain III)	
		4. Dark luminescent rims	
SI10-72—Migmatitic gt-bearing felsic gneiss	This sample comes from an isoclinally folded leucosome within a garnet-biotite-bearing gneiss (Figure 7d). This outcrop is dominated by melt (up to 40–50%) and is highly deformed. The migmatitic foliation (SP_{5a}) is folded axial planar to FP_{5b}.	Zircon grains in this sample are typically rounded and have resorbed margins. They can be up to 400 μm long and have aspect ratios of up to 3:1. The internal zircons textures as observed under CL include the following:	Majority of the zircon grains are discordant.
11°03′55.8″N 78°02′17.2″E		1. Bright to dark luminescent oscillatory-zoned cores (Figure 5d, grains I and III)	Oscillatory-zoned cores yielded discordant Archaean to Palaeoproterozoic ages.
		2. Metamict dark luminescent cores (Figure 5d, grain II)	Two concordant zircon grains yielded ages of 2928 ± 21 Ma and 3476 ± 19 Ma, attesting to the sedimentary nature of the garnet-biotite-gneiss.
		3. Ghost zoning suggesting solid-state recrystallization	Two concordant (<5% disk) sector-zoned rims (type 3) yielded a weighted average $^{206}Pb/^{238}U$ age of 538 ± 10 Ma (n = 2, 2σ, MSWD = 0.36).
		4. Sector-zoned rims (growth from anatectic melts) [*Vavra et al*., 1996]	When using a 10% discordancy cutoff, the weighted average $^{206}Pb/^{238}U$ age of the rims becomes 538 ± 7 Ma (n = 5, 2σ, MSWD = 0.93) and is here interpreted as the age of migmatization (S_1) of the gt-bt-bearing protolith.
SI10-77—Undeformed pegmatite	The undeformed pegmatite cuts across a well-foliated biotite-bearing felsic gneiss (Figure 7e). The foliation in the felsic gneiss dips moderately (~62°) to the north and is defined by thin kfs-rich melts (leucosomes) and alignment of biotite, quartz, and plagioclase minerals.	Zircon grains in the pegmatite are quite large and can be up to 1 mm long with aspect ratios of up to 3:1. They are euhedral (Figure 5e, grain IV) except when broken up during crushing. Two types of zircon grains were distinguished based on the internal textures observed under CL:	Ages obtained from type 1 zircons were mostly discordant with a single concordant (<5% disk) $^{207}Pb/^{206}Pb$ age of 2499 ± 21 Ma.
11°01′22.7″N 78°05′07.0″E		1. Bright luminescent oscillatory-zoned grains (Figure 5e, grain III)	Type 2 zircons yielded a combined weighted average $^{206}Pb/^{238}U$ age of 523 ± 6 Ma (n = 7, 2σ, MSWD = 0.78).
		2. Dark luminescent, faintly zoned large grains (Figure 5e, grains I, II and IV)	
		NEMB transect	
SI10-113—Granodioritic gneiss	This sample is a granodioritic gneiss that preserves two phases of deformation (SN_2 and SN_3). SN_2 is a migmatitic planar fabric that is parallel to the axial planes of regional-scale NE-SW trending FN_2 folds and is defined by preferential orientation of hbl-bearing	Zircon grains in this sample are quite large and can be up to 800 μm. The morphology of the grains is quite irregular with sharp terminations in some grains. It is likely that they represent fragments of a whole zircon. The internal textures observed under CL are also	The crystallization age of the protolith was obtained from a combined weighted average $^{206}Pb/^{238}U$ age of the oscillatory-zoned core analyses. They yielded an age of 789 ± 5 Ma (n = 18, 2σ, MSWD = 1.3)

Table 2. (continued)

Sample Description	Structural Evolution	Zircon Morphology and Texture Under CL	Age Interpretation and Geological Significance
	leucosomes as well as biotite, plagioclase, and quartz minerals. This fabric is overprinted by NNE trending shape fabric (SN_3) that is characterized by strain partitioning into high-strain (~10 cm) protomylonite zones and lower strain crenulated zones (Figure 9d).	somewhat irregular and variable, but majority of the zircons show well-defined oscillatory zoning. The internal textures can be summarized as follows:	
10°44′05.7″N 78°07′08.5″E		1. Oscillatory-zoned cores (Figure 5f, grains I and II)	Single concordant (0% discordant) $^{206}Pb/^{238}U$ age of 541 ± 8 Ma was obtained from a dark luminescent rim. Although it is not a statistically robust age population, it is broadly contemporaneous with the metamorphic ages obtained from migmatitic gneisses (sample SI10-72) in close proximity to it and is here interpreted as the age of metamorphism.
		2. Irregularly zoned cores with undulating zones most likely representing variable amounts of recrystallization during metamorphism (Figure 5f, grain III)	
		3. Sector-zoned rims	
		4. Dark luminescent featureless rims (Figure 5f, grain III)	
		5. Bright luminescent featureless rims (Figure 5f, grain II)	
SI10-112—Undeformed hbl-bearing pegmatite	This undeformed pegmatite cuts across (Figure 7f) the granodioritic gneiss (SI10-113, see description above) and gives an upper limit for the deformation in this domain.	Zircon grains in this sample are up to 1 mm long and have aspects ratios of up to 4:1. Some grains are irregularly shaped (due to crushing) while others are euhedral. Under CL, a number of internal zonation textures can be recognized:	U-Pb concordia yielded upper and lower intercept ages of 810 ± 60 Ma and 497 ± 27 Ma, respectively.
10°44′05.7″N E78°07′08.5″E		1. Bright luminescent oscillatory-zoned cores	The type 1 and 2 textures represent zircon cores inherited from the country rock that the pegmatite intrudes into. They yielded a weighted average $^{206}Pb/^{238}U$ age of 762 ± 7 Ma ($n = 9$, 2σ, MSWD = 1.2)
		2. Recrystallized moderately luminescent and irregularly zoned cores	Type 3 textures yielded a weighted average $^{206}Pb/^{238}U$ age of 502 ± 4 Ma ($n = 10$, 2σ, MSWD = 1.8) and are here interpreted as crystallization age of the pegmatite.
		3. Oscillatory-to sector-zoned overgrowths (rims) surrounding the bright luminescent cores (Figure 5g)	

[a]PCSS, Palghat-Cauvery Shear System, NMB, Northern Madurai Block, NEMB, North-East Madurai Block.

domain include interlayered garnet-clinopyroxene-plagioclase-bearing mafic granulites, tonalite gneisses, garnet-biotite-bearing migmatitic felsic gneisses, mylonitized magnetite-bearing quartzites, and garnet-kyanite-bearing paragneisses. Within this domain, the strain is partitioned between the higher-strain mylonitic and proto-mylonitic fabrics (SP_2) typically restricted to the felsic lithologies and the lower strain zones within the garnet-bearing mafic granulites that preserve earlier migmatitic SP_1 fabrics. The original lithological layering can be found on a meter scale and is isoclinally folded axial planar to the SP_2 fabric with moderately E plunging fold axes. The prominent L-S fabric (SP_2) is a subvertical north to south dipping gneissic to mylonitic fabric in which garnet-clinopyroxene-plagioclase mineral assemblages are

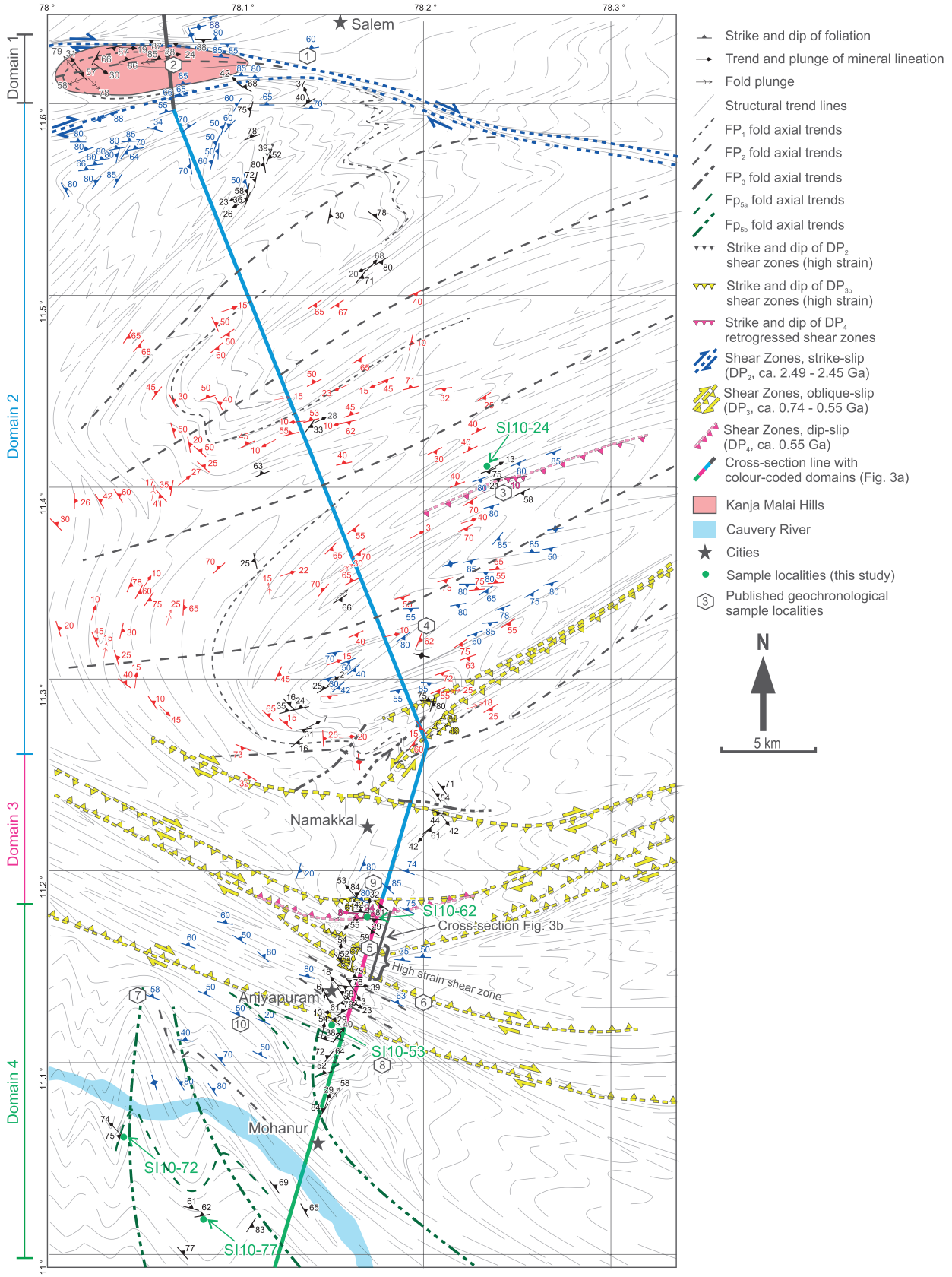
78 °
78.1 °
78.2 °
78.3 °
11.6 °
11.5 °
11.4 °
11.3 °
11.2 °
11.1 °
11 °
Domain 1
Domain 2
Domain 3
Domain 4
Salem
Namakkal
Mohanur
Aniyapuram
SI10-24
SI10-62
Cross-section Fig. 3b
High strain shear zone
SI10-53
SI10-72
SI10-77
Strike and dip of foliation
Trend and plunge of mineral lineation
Fold plunge
Structural trend lines
FP1 fold axial trends
FP2 fold axial trends
FP3 fold axial trends
Fp5a fold axial trends
Fp5b fold axial trends
Strike and dip of DP2 shear zones (high strain)
Strike and dip of DP3b shear zones (high strain)
Strike and dip of DP4 retrogressed shear zones
Shear Zones, strike-slip (DP2, ca. 2.49 - 2.45 Ga)
Shear Zones, oblique-slip (DP3, ca. 0.74 - 0.55 Ga)
Shear Zones, dip-slip (DP4, ca. 0.55 Ga)
Cross-section line with colour-coded domains (Fig. 3a)
Kanja Malai Hills
Cauvery River
Cities
Sample localities (this study)
Published geochronological sample localities
N
5 km

Figure 2

stable. The equal-area lower hemisphere projection of the measured foliations demonstrate that interpreted kilometer scale axial planar isoclinal folds associated with this fabric have moderately east plunging fold axes that are parallel to the measured mineral elongation lineations (Figure 3a). Kinematic indicators such as S-C fabrics within mylonitized magnetite-bearing quartzites (Figure 4a) and rotated garnet porphyroblasts within the garnet-bearing leucosomes (Figure 4b) show dextral movement in planes that are subparallel to the *X-Z* plane of the finite strain ellipse. Hornblende rims around garnet in the mafic granulites and biotite rims around garnet porphyroblasts suggest that the S_2 fabric is also associated with retrogression. This high-strain fabric is folded by regional to outcrop scale tight to open (FP_3) folds with steep NW plunging fold axes. Limbs of the regional FP_3 fold appear to close in the E-W direction giving an impression of a large-scale lensoid boudin enclosed by high-strain zones on either side. Some upper crustal deformation is characterized by development of small (~5 cm) brittle extensional faults, quartz ridges parallel to axial planes of FP_3 folds, and quite possibly formation of acicular muscovite grains mantling K-feldspar and plagioclase grains in the garnet-bearing paragneisses.

4.1.2. Domain 2

Domain 2 makes up the bulk of the PCSS transect and is characterized by the predominantly folded gneissic terrain between the Moyar-Salem-Attur shear zone and the Cauvery shear zone (Figure 2). The main lithologies encountered in Domain 2 include dismembered mafic and ultramafic gneisses, hornblende-bearing migmatitic gneisses, granitic orthogneisses, and high-grade metasedimentary rocks.

The primary lithological layering is hard to distinguish in most areas due to the overprinting high-grade fabric (SP_1). The earliest fabric (SP_1) is associated with partial melting and development of gneissic fabrics as well as outcrop and regional-scale isoclinal folds (FP_1, Figure 4c,). Mineral elongation lineations are variable due to the overprinting SP_2 fabric. Garnet-clinopyroxene-plagioclase mineral assemblages appear to be stable during this phase (Figure 4c) but were variably retrogressed during later deformational events (DP_2). The SP_1 fabric was overprinted by regional-scale NE-SW trending open to tight folds (FP_2) with doubly plunging fold axes (Figure 2). In the northern part of Domain 2, the variably dipping gneissic SP_1 fabric is transposed by NE plunging upright open folds, cm-scale, melt-induced NNE and WNW trending conjugate microshears, and cm-scale NW dipping dextral shears (Figure 4e). In the midsection of Domain 2, the gneissic foliation (SP_1) dips moderately to the NE and SW and becomes steeply SE dipping closer to the Cauvery shear zone (Figure 2). The variably dipping foliation defines kilometer scale upright to inclined open folds that become progressively more asymmetric and tighter toward the southern margin of this domain. The equal-area lower hemisphere projections of foliation data indicate that the interpreted fold axes of the regional-scale folds (Figure 3a) plunge gently (~16°) to the NE. The moderately (~10–50°) NE and SW plunging mineral elongation lineations are subparallel to FP_2 fold axes (Figure 3a) and suggest that folding was accompanied by extension parallel to fold hinges. Mesoscale axial planar hornblende-orthopyroxene-bearing leucosomes pass into the conjugate microshears suggesting that partial melts were still present during this deformation (DP_2). Boudinaged mafic layers and leucosome-filled boudin necks indicate a significant component of layer-parallel extension while rotated mafic boudins at some localities (e.g., 11°32′24.0″N, 78°10′39.8″E) preserve the SP_1 foliation

Figure 2. Structural map across the Palghat-Cauvery Shear System (PCSS). Blue colored structural readings were obtained from *Ghosh et al.* [2004]; red structural readings were obtained from *Chetty and Bhaskar Rao* [2006a], and black structural readings were obtained during this study. Structural trends were defined through field observations coupled with satellite imagery. U-Pb zircon and monazite ages obtained by other authors are given by numbered polygons: (1) Sample S-27, 2527 ± 4 Ma crystallization age of a granitic gneiss [*Ghosh et al.*, 2004]; (2) Kanja Malai locality, circa 2.65–2.5 Ga detrital zircon spectra [*Anderson et al.*, 2012; *Plavsa et al.*, 2014], circa 2.5 Ga protoliths [*Saitoh et al.*, 2011; *Sato et al.*, 2011b], HP-HT metamorphism (14–16 kbar, 820–850°C) [*Anderson et al.*, 2012]; (3) Sample S-220, intrusion of biotite gneiss into mafic granulite 2512 ± 2 Ma [*Ghosh et al.*, 2004]; (4) Sample S-130, zircon crystallization ages of 2525 ± 20 Ma and 2507 ± 1 Ma (interpreted metamorphic age) [*Ghosh et al.*, 2004]; (5) Sample SI10-71, garnet-bearing leucocratic gneiss (detrital zircon dating), 2.55–2.45 Ga protoliths, Pb loss to circa 740 Ma [*Plavsa et al.*, 2014]; (6) Sample S-117, mafic granulite near Namakkal, circa 2.5 Ga and 2.9 Ga ages from rim and cores of zircon, respectively, and 722 ± 13 Ma younger anhedral zircon population [*Ghosh et al.*, 2004]; (7) Panangad locality analyzed by *Collins et al.* [2007a] and *Clark et al.* [2009a]. Zircon cores from a mafic gneiss yielded discordant Archaean to Paleoprotereozoic ages, rims, and multifaceted metamorphic zircon yielded ages circa 535 Ma and monazite ages circa 525 Ma ($P > 12$ kbar, T ~950°C). (8) Sevitturanganpatti locality [*Clark et al.*, 2009a; *Collins et al.*, 2007a], 535 Ma metamorphic zircon ages, 532 Ma, and 525 Ma monazite ages from a garnet-corundum-kyanite-gedrite-sapphirine mafic gneiss and sillimanite-muscovite-quartz schist, respectively; (9) garnet-clinopyroxene-plagioclase-ilmenite mafic granulite (sample I-20-1-07) with circa 2.6 Ga inheritance, crystallization age of 2502 ± 8 Ma, and a metamorphic overprint at 2486 ± 16 Ma and a younger lower intercept of 804 ± 16 Ma [*Brandt et al.*, 2014], suggesting some Pb loss during the early Neoproterozoic; and (10) migmatitic biotite-bearing gneiss (sample I-24-1-07) with upper and lower intercepts of 823 ± 26 Ma and 534 ± 45 Ma (MSWD = 0.83) with the upper intercept here interpreted as the crystallization age and the lower intercept indicating metamorphism and Pb loss during the Cambrian [*Brandt et al.*, 2014].

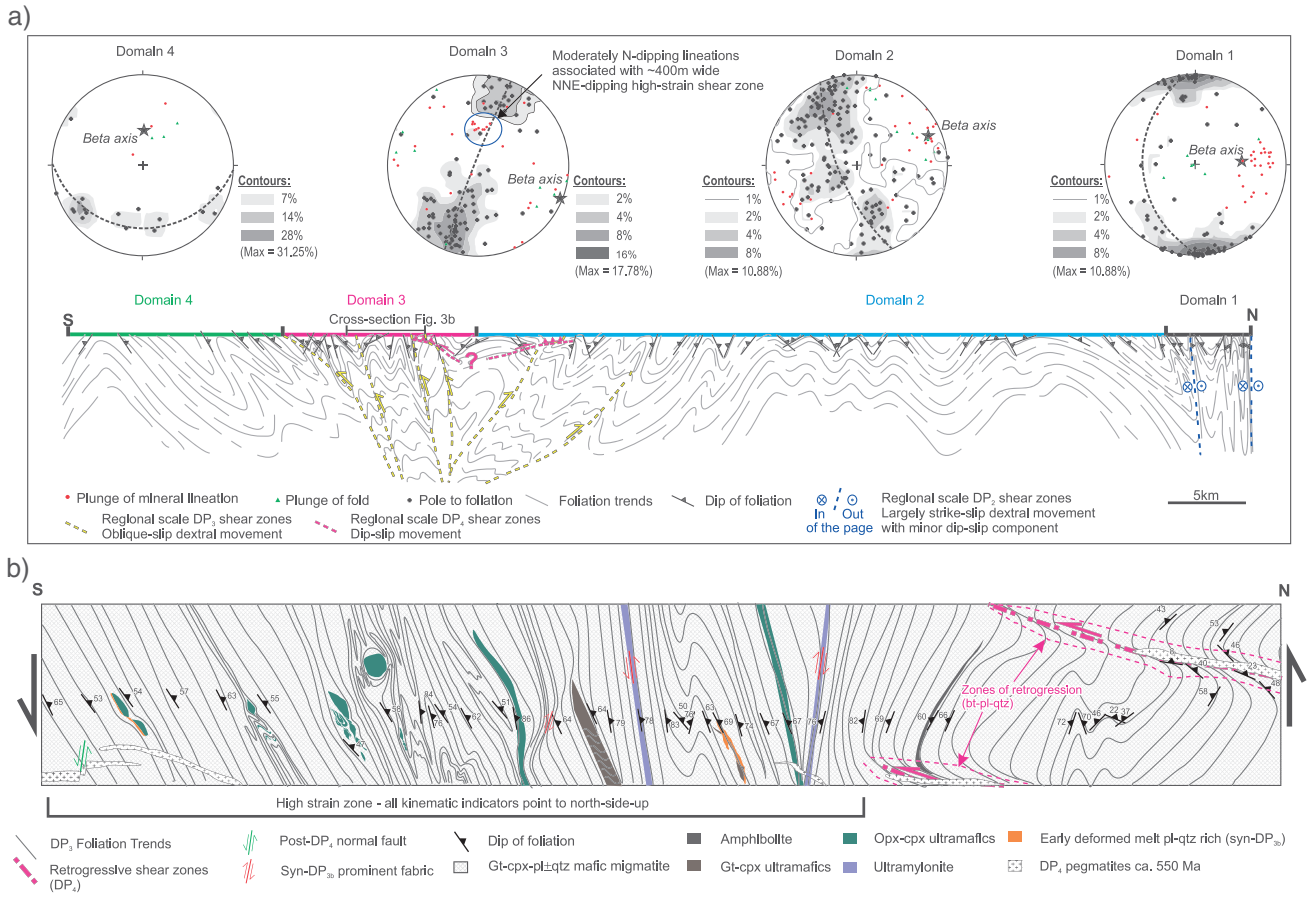

Figure 3. Cross-sectional map of the Palghat-Cauvery Shear System transect from north to south: (a) Regional-scale cross-sectional map of the Palghat-Cauvery Shear System and (b) schematic cross section of Domain 3–Cauvery shear zone (interpreted as a Neoproterozoic suture zone).

discordant to the pervasive high-strain SP_2 fabric. In the lower strain domains (usually in the more competent garnetiferous mafic gneisses), the overprinting fabrics of SP_2 on SP_1 are best observed. At one such locality (11°33′50.1″N, 78°06′35.3″E), a moderately west dipping S_1 gneissic fabric is overprinted by a NE-SW trending S_2 shape fabric defined by reorientation of plagioclase and quartz minerals in the leucocratic layers as well as clinopyroxene and garnet aggregates. Hornblende forms rims around clinopyroxene grains and is common elsewhere in the finer-grained matrix quite possibly indicating decompression during SP_2. Toward the southern margin of Domain 2, moderately (~50°) SSE dipping shear zones (Figure 2) and ENE-WSW trending shape fabrics (SP_3) overprint the high-grade $SP_{1/2}$ (SP_1/SP_2) fabrics and are characterized by realignment of clinopyroxene-plagioclase-quartz minerals in a garnet-clinopyroxene-bearing gneiss. The lower strain domains between the SP_3 shear zones are folded by upright moderately SE plunging folds (FP_3). Finally, shallow (~10°) high-strain S dipping shear zones up to 30 m thick cut across the layered mafic-ultramafic sequences and cause significant retrogression of metagabbros to hornblende-plagioclase-bearing assemblages. The fabric associated with this late shear zone (SP_4) is an L-S fabric with a better developed mineral elongation lineation defined by stretched plagioclase and hornblende minerals that plunge gently to the east. Large (up to 3 m) unretrogressed pyroxenite boudins are wrapped by the SP_4 shear fabric (Figure 4f), but the sense of movement was not discernible. However, the moderate SSE (~50°) $SP_{1/2}$ foliation dips curve into the SP_4 shear and suggest that the dip-slip component along this shear indicates south side-up movement.

A biotite-bearing granodioritic gneiss (SI10-24, Figure 2 and Table 2) containing pyroxenite enclaves and preserving the NE-SW trending foliation ($SP_{1/2}$) was dated using U-Pb zircon geochronology to constrain the timing of crystallization and metamorphism. Six concordant (≤5% discordant) oscillatory-zoned cores

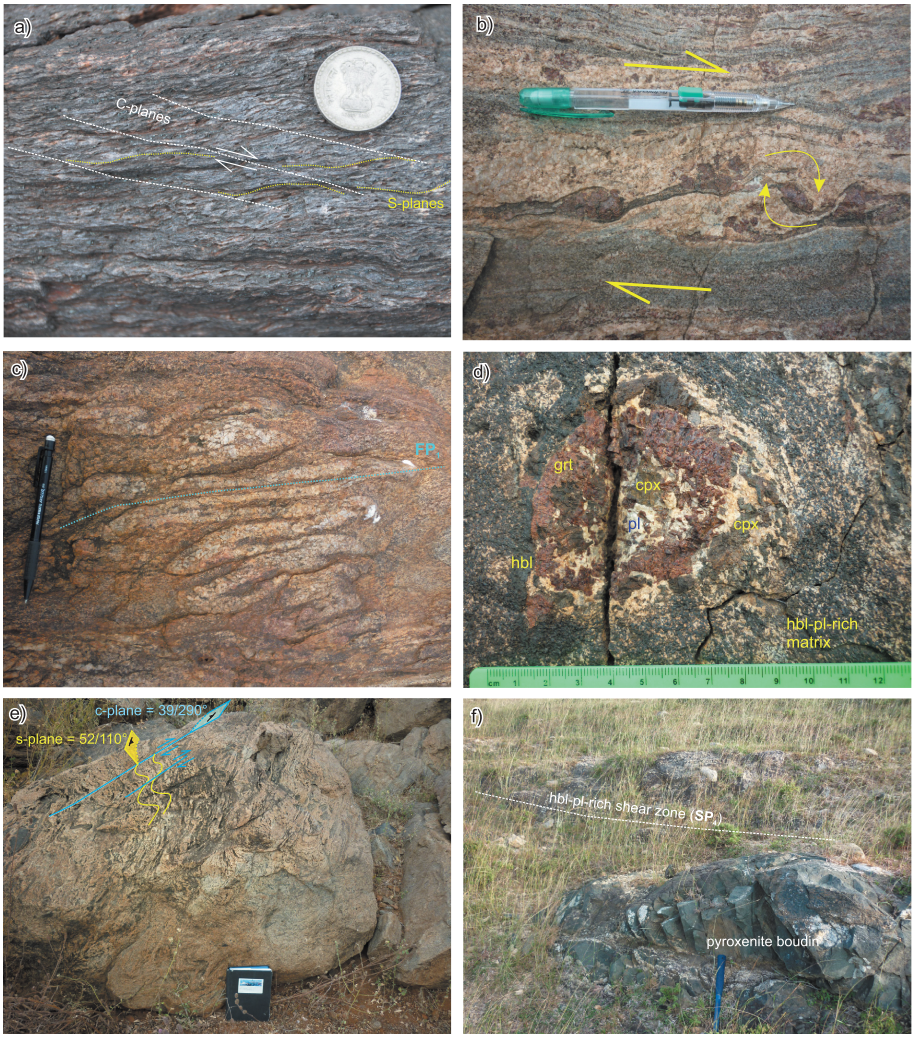

Figure 4. Field photographs of the main deformational fabrics and mineral assemblages in Domain 2, PCSS transect: (a) photo looking south, C-S fabrics (SP_2) associated with dextral strike-slip movement in mylonitized magnetite-bearing quartzites at Kanja Malai Hills; (b) photo looking south, rotated garnet porphyroblasts in leucosomes showing dextral kinematics subparallel to the *X-Z* plane of the finite strain ellipse; (c) photo looking NW, isoclinally folded leucosomes associated with development of early SP_1 fabrics; (d) coarse-grained garnet-clinopyroxene-plagioclase mineral assemblages surrounded by a corona of hornblende and imbedded in hbl-pl-cpx-rich matrix interpreted to represent retrogression during DP_2; (e) NW dipping, cm-scale dextral shears folding the early SP_1 gneissic fabric; and (f) pyroxenite boudins wrapped by hbl-pl-rich shear zone with prominent mineral elongation lineation.

yield a weighted average $^{207}Pb/^{206}Pb$ age of 2534 ± 17 Ma (2σ, MSWD = 1.17). The bright luminescent outer and sector-zoned inner rims along with bright luminescent sector-zoned zircons (Figure 5a) yielded a weighted average $^{207}Pb/^{206}Pb$ age of 2501 ± 13 Ma (n = 15, 2σ, MSWD = 1.6, Figure 6a), here interpreted as dating metamorphism.

4.1.3. Domain 3

This domain encompasses the high-strain domain typically defined as the Cauvery shear zone [*Chetty and Bhaskar Rao*, 2006b; *Santosh et al.*, 2009] that is interpreted by many workers to be the site of a strand of the Mozambique Ocean that closed here at circa 550–500 Ma [*Collins and Pisarevsky*, 2005; *Santosh et al.*, 2006; *Collins et al.*, 2007a; *Clark et al.*, 2009b; *Santosh et al.*, 2009; *Yellappa et al.*, 2010; *Sato et al.*, 2011a; *Santosh et al.*, 2012]. It extends from the town of Namakkal to immediately north of the town of Mohanur (Figure 2). Unlike in Domain 2, the lithological units that make up the bulk of Domain 3 are garnet-clinopyroxene-plagioclase ± quartz mafic granulites and their retrogressed equivalents, clinopyroxene-orthopyroxene and garnet-clinopyroxene pyroxenites and dunites, garnet-bearing

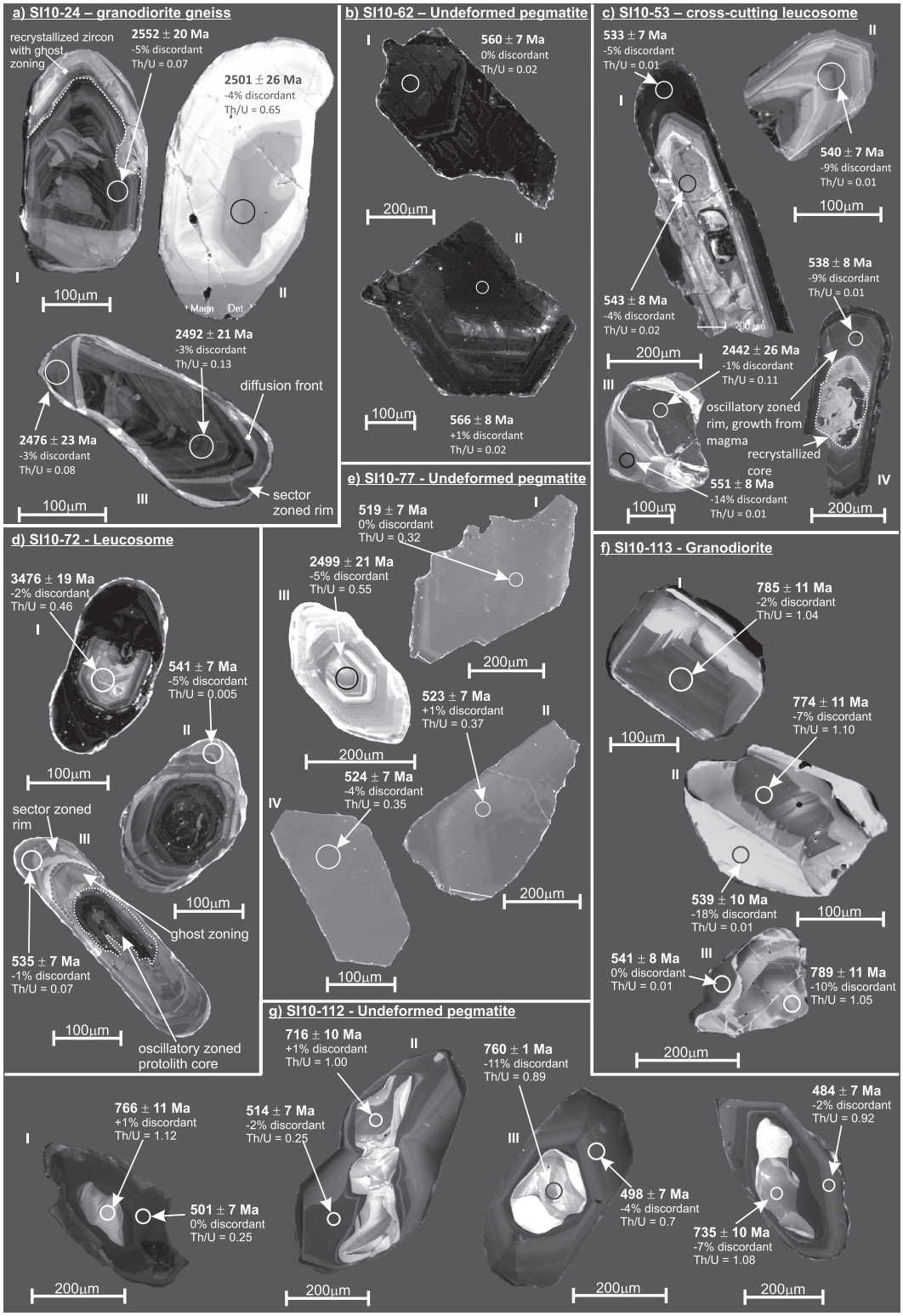

Figure 5. Cathodoluminescence (CL) images of the analyzed zircon grains and corresponding U-Pb ages. The quoted ages are $^{207}Pb/^{206}Pb$ for analyses >1000 Ma and $^{206}Pb/^{238}U$ for analyses <1000 Ma.

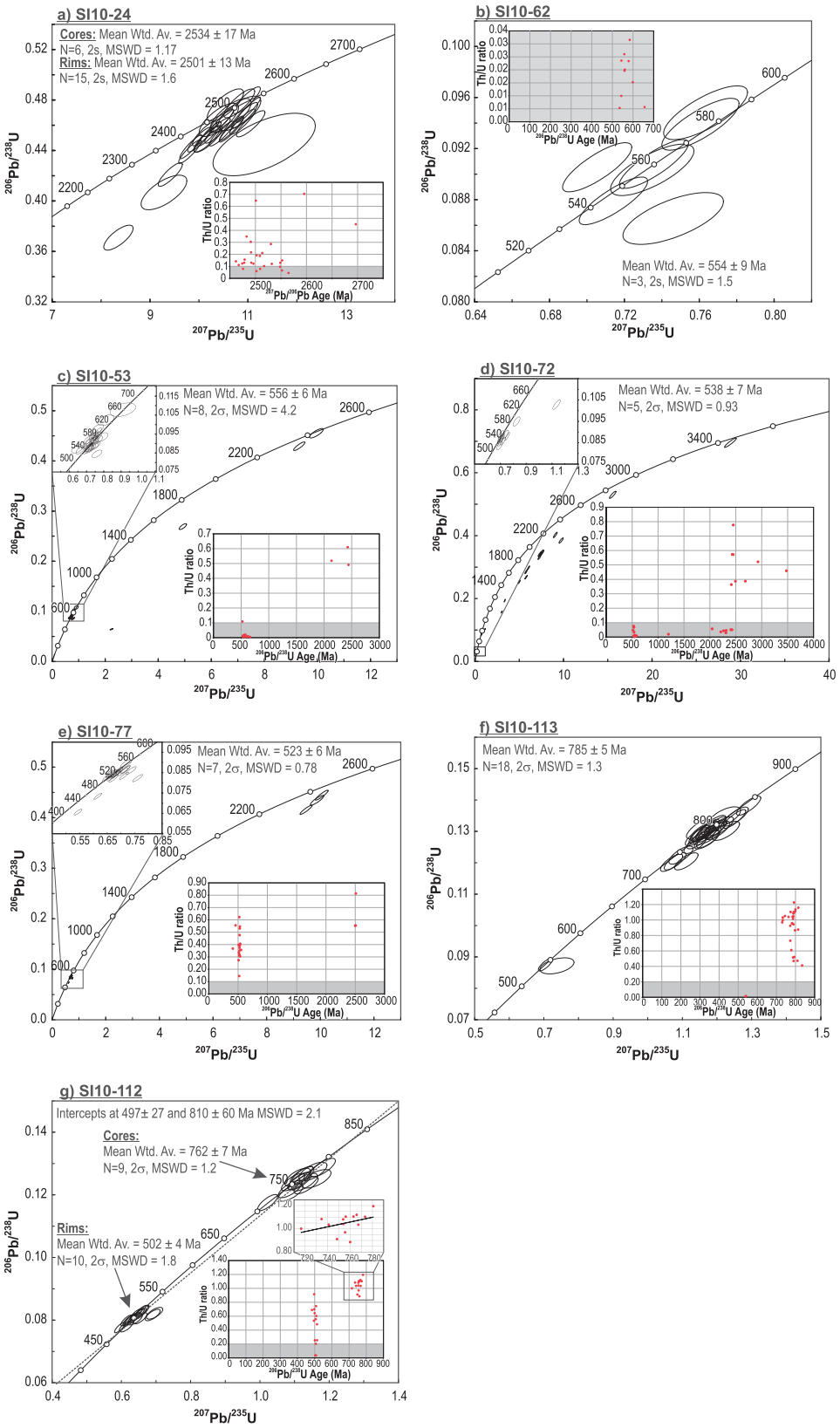

Figure 6. (a–g) U-Pb concordia plots of the analyzed samples in this study. The inset figures show Th/U versus Age (Ma) plots of the corresponding analyses. Grey area in the inset photos depicts Th/U ratios of <0.1 suggestive, but not conclusive, of metamorphic origins [*Hoskin and Black*, 2000]. The quoted mean weighted average ages are $^{206}Pb/^{238}U$ for ages <1000 Ma and $^{207}Pb/^{206}Pb$ for ages >1000 Ma.

leucocratic ultramylonites, metachert interlayered with garnet-clinopyroxene-plagioclase-quartz mafic granulites, and crosscutting pegmatites. Lithological and structural relationships of this domain are best observed in well-exposed fresh outcrops in a railway cutting between Namakkal and Aniyapuram (Figure 2). This transect exposes a section perpendicular to the main foliation trend, and a schematic cross section (Figure 3) shows the main structural relationships. The strain in this domain is much higher than that of Domain 2 and is characterized by grain size reduction (average grain size between 3 and 5 mm) with occasional garnet porphyroblasts of up to 7–10 cm in diameter, typically preserved in the lower strain domains. The primary lithological layering was not observed due to the pervasive overprinting high-grade (SP_{3a} and SP_{3b}) fabrics. The earliest fabrics (SP_{3a}) are associated with the development of gneissic layering that is characterized by 1–2 cm thin garnet-clinopyroxene ± plagioclase mafic bands and slightly thicker (up to 5 cm) plagioclase-clinopyroxene ± quartz felsic bands. Significant differentiation and melting occurred at this time leaving behind garnet-clinopyroxene-rich restites with minor interstitial plagioclase as well as plagioclase-rich leucosomes that were overprinted by SP_{3b} fabrics. Lineations are difficult to reconcile due to the overprinting SP_{3b} fabrics. The pervasive SP_{3b} fabric is characterized by the lower strain fold-dominated and higher-strain mylonite-dominated domains. Starting at the northern end of the cross section (Figure 3b), this fabric is axial planar to open upright symmetric folds (FP_{3b}) and shallow plunging (~5–15°) ESE-WSW fold axes. The measured mineral elongation lineations are subparallel to the FP_{3b} fold plunges, suggesting extension parallel to fold hinges (Figure 3a). Plagioclase, clinopyroxene, and quartz within the SP_{3a} gneissic fabric and the syntectonic plagioclase-quartz-rich leucosomes are progressively reoriented to be axial planar to FP_{3b} folds and toward parallelism with the mylonite zone farther south. Furthermore, hornblende-bearing leucosomes crosscut the earlier SP_{3a} gneissic fabrics in an orientation parallel to the axial planes of FP_{3b} folds. The ~400 m high-strain zone is characterized by steeply (~50–85°) NNE dipping mylonites (grain size reduction to ~1–3 mm) and moderately N dipping mineral elongation lineations (Figure 3a). The kinematic indicators showing north block-up (dextral) movement are abundant in the high-strain mylonite zone where they are observed subparallel to the *X-Z* plane of the strain ellipsoid (Figure 3b). The kinematic indicators include (1) cm-scale S-C fabrics with moderately (~40°) N dipping plagioclase-quartz dominated C planes and steeply N dipping garnet-clinopyroxene-plagioclase-bearing S planes; (2) centimeter to meter scale pyroxenite boudins forming σ clasts; (3) meter scale foliation lozenges (Figure 3b). At the southern margin of Domain 3, the SP_{3a} gneissic foliation is folded by tight to isoclinal south verging ESE-WSW shallow plunging folds (FP_{3b}) with mineral elongation lineations subparallel to the fold hinges. The axial planes of FP_{3b} folds dip moderately to steeply (~50–70°) to the NNE (Figure 3a) and most likely represent a lower strain equivalent of the north block-up movement observed in the mylonite zone farther north. The similarity in structural orientations of the fold axes and mineral lineations of the open upright folds in the northern part of Domain 3 and tight to isoclinal folds farther south suggests that they are contemporaneous with the north block-up movement. The latest deformational phase (D_4) is associated with structurally controlled retrogression linked to pegmatite intrusions. Large-scale (up to 5–10 m) shallow (~10–30°) N dipping recumbent folds (FP_4) with attenuated (sheared) lower limbs deform the earlier SP_{3a} and SP_{3b} fabrics via grain size reduction and retrogression of clinopyroxene-garnet-plagioclase mafic gneisses to biotite-hornblende-bearing assemblages. The folded SP_{3b} fabrics and sheared lower limbs give impression of large-scale C-S relationships with north block-up sense of movement (Figure 7a). Fold hinges of FP_4 folds plunge gently (~10–20°) to the west. Thick (up to 2 m thick) pegmatites (sample SI10-62) intrude along the sheared limbs and are most likely responsible for the retrogressive aureoles associated with these shears (Figure 7b). Small-scale (~20 cm) shallow N dipping reverse faults cutting across the mylonite zone and shallow N dipping fracture cleavage planes farther south are considered contemporaneous with DP_4 deformation. No new mineral growth or reorientation of preexisting mineral is associated with this phase, suggesting that this deformation took place in upper crustal levels during formation of low-angle thrusts.

A sample of the crosscutting pegmatite (sample SI10-62, Figures 6b and 7b) was dated using U-Pb zircon geochronology. The zircon grains were typically dark under CL (Figure 5b) and show evidence of damage due to radiation damage resulting from the high concentrations of Th and U. The zircon grains show a range of concordant dates ranging between circa 580 and 540 Ma (Figure 6b) with three concordant (≤5% discordant) oscillatory-zoned grains yielding a weighted average $^{206}Pb/^{238}U$ age of 554 ± 9 Ma (Figure 6b), here interpreted as the crystallization age of the pegmatite.

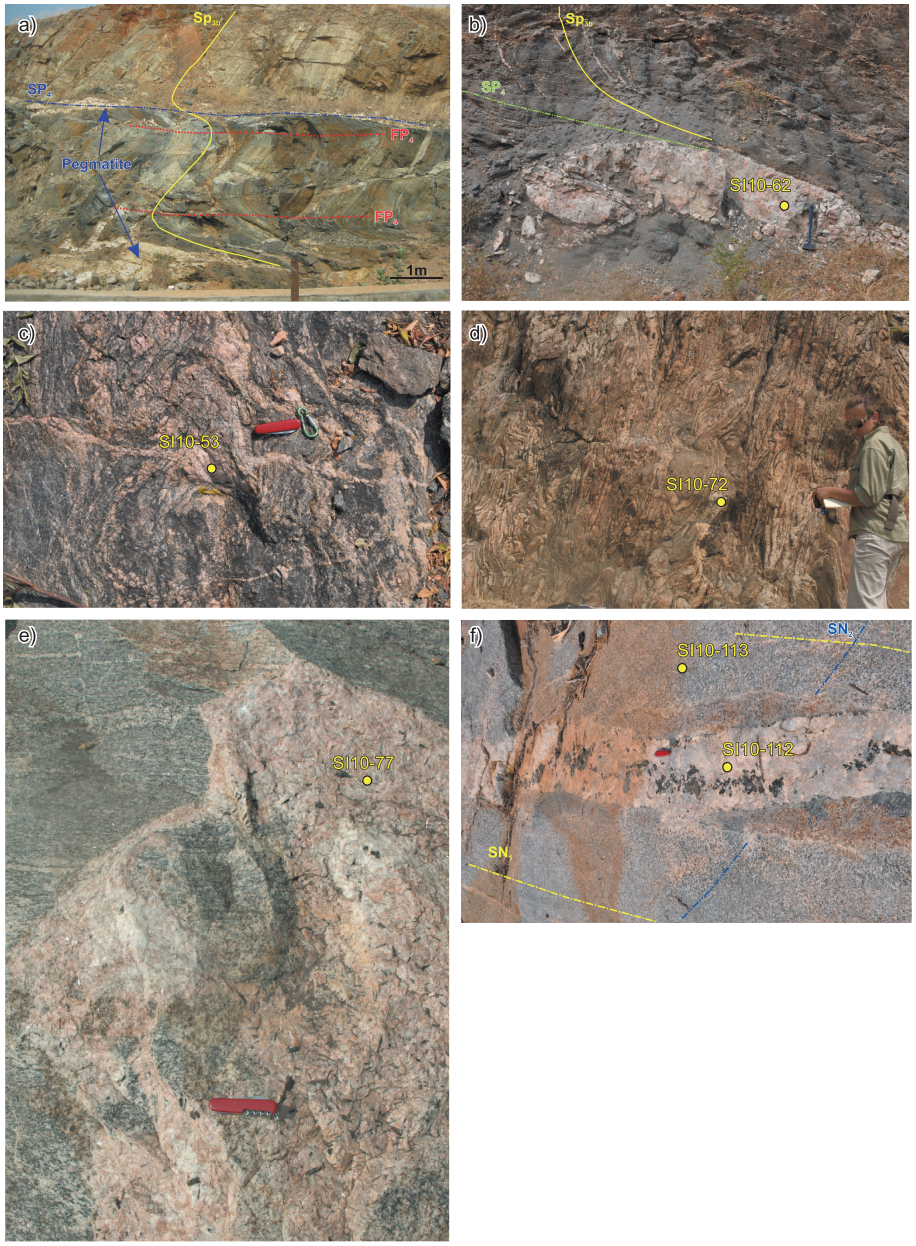

Figure 7. Field photos of the deformation style and samples analyzed in this study: (a) photo looking west, retrogressed mafic granulites in the Cauvery shear zone intruded by shallow north dipping pegmatites; (b) photo looking west, high-strain fabrics (SP_{3b}) within the Cauvery shear zone recumbently folded (FP_4) with lower sheared limbs that act as conduits for pegmatite intrusions (sample SI10-62); (c) charnockitic migmatite immediately south of the Cauvery shear zone cut by a thin leucosome (sample SI10-53); (d) isoclinally folded garnet-bearing granitic migmatite Domain 4, Palghat-Cauvery Shear System transect, immediately south of the Cauvery shear zone (sample SI10-72, leucosome); (e) undeformed pegmatite (sample SI10-77) cuts across a migmatitic biotite-bearing felsic gneiss immediately south of the Cauvery shear zone; and (f) granodioritic gneiss (sample SI10-113) recording two (and possibly three) phases of deformation (DN_1 and DN_2/DN_3) in the Northern Madurai Block within the NE Madurai Block transect, crosscut by an undeformed hornblende-bearing pegmatite (sample SI10-112).

4.1.4. Domain 4

This domain is located immediately south of the Cauvery shear zone (Domain 3) and marks the northernmost margin of the Madurai Block. There is a major lithological boundary between Domains 3 and 4 marked by the decrease in Mg-Al rich mafic gneisses to largely potassic K-feldspar-biotite-garnet-bearing migmatites. Primary lithological relationships were not observed in this domain due to the highly

migmatized nature of the protoliths. At the northernmost margin of Domain 4, the dominant rock units are hornblende-biotite-bearing and garnet-hornblende-biotite-bearing migmatites defined by alternating leucosome (K-feldspar-plagioclase-quartz) and mesosome (hornblende-biotite-plagioclase with or without garnet) layers (Figures 7c and 7d). Two phases of metaigneous rocks are recognized with early migmatitic clinopyroxene-bearing (charnockitic) orthogneisses and later granodioritic biotite-bearing felsic gneisses that preserve only steeply (~70°) NE and NW dipping SP_{5a} fabrics. The migmatite layers (SP_4) are isoclinally folded and brought into parallelism with the axial planes of FP_{5a} folds thus giving rise to the predominant L-S planar fabric (SP_{5a}) in this domain (Figure 7d). Thin (2–19 cm) leucosomes locally cut across the main SP_4 fabric (sample SI10-53, Figure 7c) and intrude along the axial planes of FP_{5a} folds (sample SI10-72, Figure 7d), suggesting some partial melt was available during, and perhaps immediately after, the deformation. The orientation of the SP_{5a} foliation is variable due to later refolding (FP_{5b}) but dips moderately (~30–45°) to the NE and NW immediately south of the Cauvery shear zone and becomes progressively steeper (~50–85°) with similar orientations toward the south. The SP_{5a} fabric is folded by steeply (~50–60°) NNE plunging open folds (FP_{5b}). Mineral elongation lineations defined by the alignment of biotite laths plunge moderately to steeply (~30–75°) to the north and are subparallel to the FP_{5b} fold axes. Centimeter scale (~2 cm) shear bands dipping moderately (~40°) to the NW cut across the SP_{5a} fabrics and show sinistral sense of movement observed in horizontal planes. Small-scale asymmetric folds between the shear bands plunge ~40° to the NE and are subparallel to the interpreted regional-scale FP_{5b} folds (Figure 3a). All fabrics are crosscut by thick (~1 m thick) biotite-bearing pegmatites (sample SI10-77, Figure 7e).

Zircon grains from the crosscutting thin granitic veins (sample SI10-53) show featureless moderately luminescent to completely recrystallized protolith cores mantled by oscillatory- to sector-zoned rims (Figure 5c and Table 2). The concordant (<5% discordant) analyses of the oscillatory-zoned overgrowths yielded a range of $^{206}Pb/^{238}U$ ages between circa 660 and 530 Ma (Figure 6c), with a combined weighted average $^{206}Pb/^{238}U$ age of 556 ± 6 Ma ($n = 8$, 2σ, MSWD = 4.2), here interpreted as the crystallization age of the granitic melt. The analyses of the recrystallized and featureless cores yielded largely discordant Archean ages with two concordant analyses (≤5% discordant) yielding $^{207}Pb/^{206}Pb$ ages of 2428 ± 22 Ma and 2442 ± 26 Ma, here interpreted as inheritance from the migmatized protoliths.

Zircon grains from the granitic melts intruding along the axial planes of FP_{5b} folds (sample SI10-72) show oscillatory-zoned and metamict dark luminescent cores surrounded by thick (up to 150 μm, grain III, Figure 5d) sector-zoned rims. The oscillatory-zoned cores yielded a range of discordant Archean ages (Figure 6d) with a single concordant $^{207}Pb/^{206}Pb$ age of 3476 ± 19 Ma (2% discordant), here interpreted as dating the age of xenocrystic zircons inherited from the adjacent gneiss. Five concordant (≤10% discordant) sector-zoned overgrowths yielded a combined weighted average $^{206}Pb/^{238}U$ age of 538 ± 7 Ma (2σ, MSWD = 0.93) that is interpreted as the crystallization age of the granitic vein.

The zircon grains from the late crosscutting pegmatite (SI10-77, Figure 7e) are typically large (up to 1 mm), dark luminescent and faintly oscillatory-zoned under CL (Figure 5e, grains I, II, and IV) with occasional bright luminescent oscillatory-zoned zircons present (Figure 5e, grain III). The concordant (≤5% discordant) dark luminescent oscillatory-zoned grains yielded a weighted average $^{206}Pb/^{238}U$ age of 523 ± 6 Ma ($n = 7$, 2σ, MSWD = 0.78) here interpreted as crystallization age of the pegmatite. The bright luminescent oscillatory-zoned cores yielded largely discordant Archean ages (Figure 6e), with a single concordant (≤5% discordant) $^{207}Pb/^{260}Pb$ age of 2499 ± 21 Ma, here interpreted as inheritance from the surrounding rocks.

4.2. North-East Madurai Block

This transect is located immediately to the south of the Cauvery shear zone and has similar structural and lithological character to Domain 4, but different to that of Domains 1–3, of the PCSS transect (see Table 4 for the summary of main deformational events and correlative nomenclature between the structural transects). The structural transect extends over ~50 km in a N-S direction and covers all of the major lithologies that dominate the north eastern part of the Madurai Block. The majority of the area is flat lying, and at times outcrops are hard to find due to the thick lateritic weathering. Nevertheless, a number of overprinting fabrics were recognized on an outcrop and regional scale. As previously described by many authors [*Drury et al.*, 1984; *Ghosh et al.*, 2004; *Cenki and Kriegsman*, 2005; *Santosh et al.*, 2009] the flat-lying

areas in the Madurai Block are dominated by migmatites (hornblende-biotite bearing and garnet bearing), metasedimentary units including marbles, calc silicates, and garnet-biotite schists, while the strongly foliated quartzites form distinct ridges mantling gabbroic intrusions (e.g. the Kadavur Dome) [*Teale et al*., 2011; *Kooijman et al*., 2011].

The regional-scale patterns (Figure 8), as well as stereonet projections of the high-strain fabrics, give evidence for a polydeformational history, including refolded folds and variably oriented mineral elongation lineations. The most prominent structural fabrics are NE-SW trending and become progressively deflected toward NNE-SSW trends farther south. A prominent high-strain zone extending from Muthampatti to Palayam and Eriyodu (MPE, up to 2 km thick, Figure 8) is also deflected from NE-SW to NNE-SSW to the south. The regional structural patterns including asymmetric folds and deflection of fabrics into the high-strain zone suggest opposing movements between NE-SW trending fabrics (dextral) and NNE-SSW fabrics (sinistral). The detailed description of structural features observed in outcrops is given below.

The primary lithological relationships between different units were not observed in the majority of the NE Madurai Block transect due to the overprinting high-grade fabrics. The original lithological layering (SN_0) in this domain was only observed in quartzites where it was defined by the heavy mineral laminations. At the northern margin of the North-East Madurai Block (NEMB) transect, the predominant lithological units are granitic (sometimes garnet bearing) to granodioritic migmatitic gneisses interlayered with amphibolites. The contacts between these units are concordant to the dominant migmatitic planar fabric (SN_1) that is axial planar to isoclinal FN_1 folds and often defined by layer-parallel leucosomes and alternating leucocratic and mafic bands. At the northern end of the NEMB transect, this fabric dips steeply to the NNW (~50–80°). At one locality (10°49′36.7″N, 78°7′25.5″E), an amphibolite unit in contact with a more felsic granodioritic gneiss is defined by subvertical NNW dipping planar fabric (SN_1) that is overprinted by steep NE-SW trending (~040°) shape fabric (SN_2). The late SN_2 fabric is also associated with discontinuous plagioclase-quartz-rich leucosomes with preferred NE-SW orientations (Figure 9a). Within the felsic migmatitic gneisses in close proximity to the amphibolite units, two generations of leucosomes can be recognized including those parallel to the high-strain SN_1 fabric (subvertically NNE dipping) and those crosscutting the fabric in the NE-SW orientation (~040–070°). The second generation leucosomes are typically associated with cm-scale sinistral shears as observed in the horizontal planes. The regional structural pattern is defined by post-SN_1 folding (FN_2) with NE-SW trending axial planes and variably plunging mineral lineations. The DN_2 event is most likely contemporaneous with SN_2 shape fabrics observed in the amphibolites and late crosscutting leucosomes. Farther south along the transect, near the contact with the calc-silicate metasedimentary rocks (Figure 8), the folding of the SN_1 fabric on a regional and outcrop scale becomes more obvious with mineral lineations also folded by FN_2 folds. The FN_2 folding is most obvious in the calc-silicate metasedimentary rocks where it forms open upright folds with gentle (~10–20°) NE plunging fold axes (Figure 9b). The high-grade fabric (SN_1) in the calc-silicate metasedimentary rocks is defined by thin (1–3 cm) calcite-rich and silica-rich alternating bands. At one locality (10°41′55.2″N, 78°14′40.6″E), this high-grade fabric is axial planar to isoclinal folds (FN_1) that are parallel to the lithological banding within the calc-silicate units (Figure 9c). Silica-rich bands are often boudinaged and dismembered throughout the marble dominated layers, and it is not clear whether this is associated with extension parallel to fold axes during FN_2 folding or whether it was a product of the earlier high-strain planar fabric (SN_1). Boudins of granitic gneiss within the calc-silicate metasedimentary rocks show layer-parallel extension with melt filling the necks of the boudins. On a regional scale, the calc-silicate units define a synform with NE plunging fold axis. Within the hinge of the fold, strongly foliated granodioritic gneisses (sample SI10-113, Figure 7f) with layer-parallel calc-silicate enclaves commonly display two fabrics. The first fabric (SN_1) is defined by mineral and leucosome (hornblende bearing) preferred orientations (Figures 7f and 8d) and has a subvertical SE dip. On the regional scale, this early fabric appears to be parallel to the axial plane of FN_2 folds. This early SN_1 fabric is cut by thin (~5 cm) granitic veins that are asymmetrically folded by late NNE-SSW trending fabric (SN_2, Figure 9d). The SN_2 fabric in the granodioritic gneiss is heterogeneous and defined by higher-strain zones (~10 cm) with strong mineral preferred orientations and lower strain zones where it is associated with microscale (~1–2 cm) folds producing small-scale crenulations of the SN_1 fabric. Both fabrics are crosscut by undeformed pegmatites with large (up to 5 cm) euhedral hornblendes (sample SI10-112, Figure 7f). Directly south of

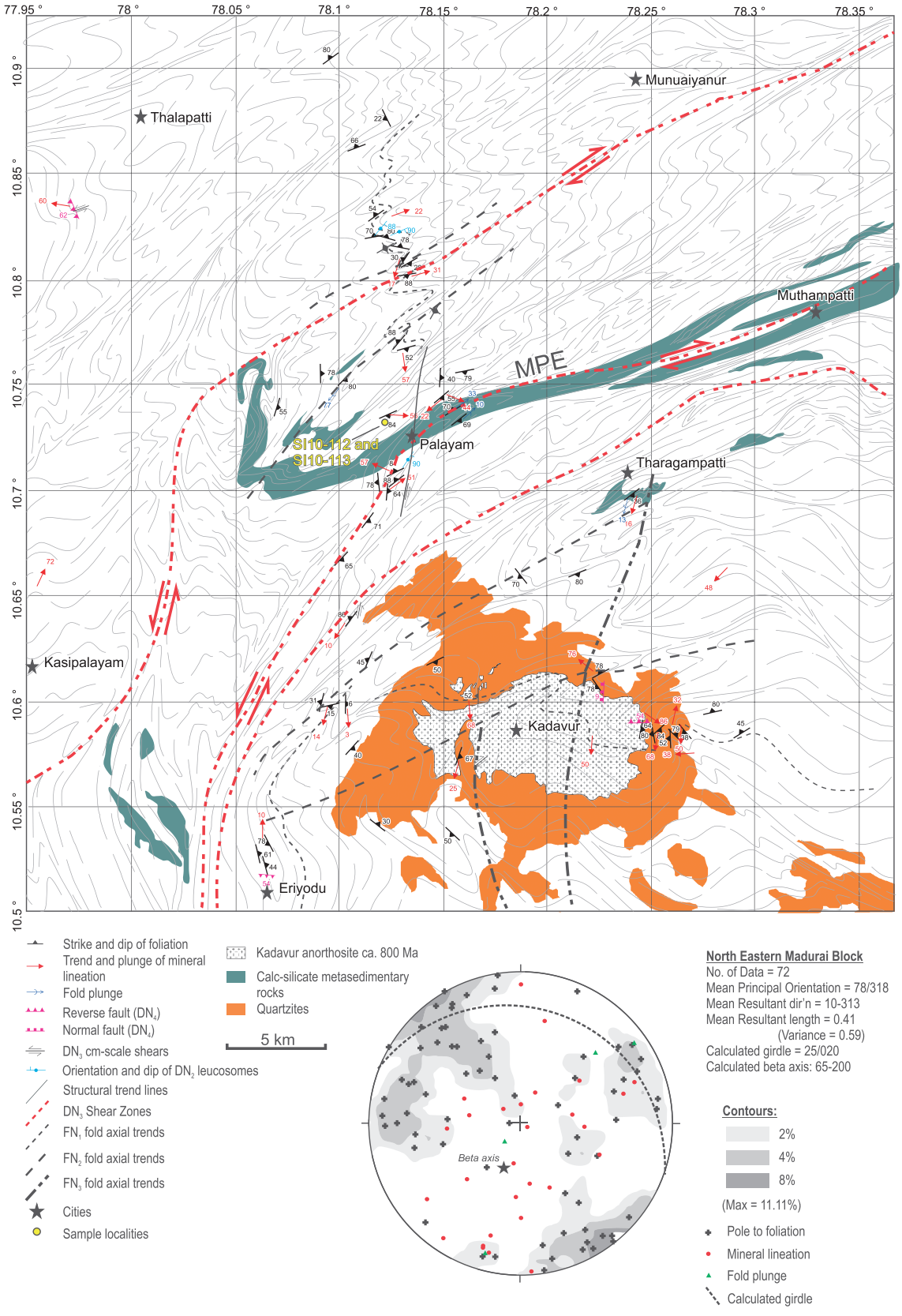

Figure 8. Structural map of the North Eastern Madurai Block transect and the equal-area lower hemisphere stereonet projection of the measured structural data. Structural trends were defined through field observations coupled with satellite imagery. MPE = Muthumpatti-Palayam-Eriyodu high-strain zone.

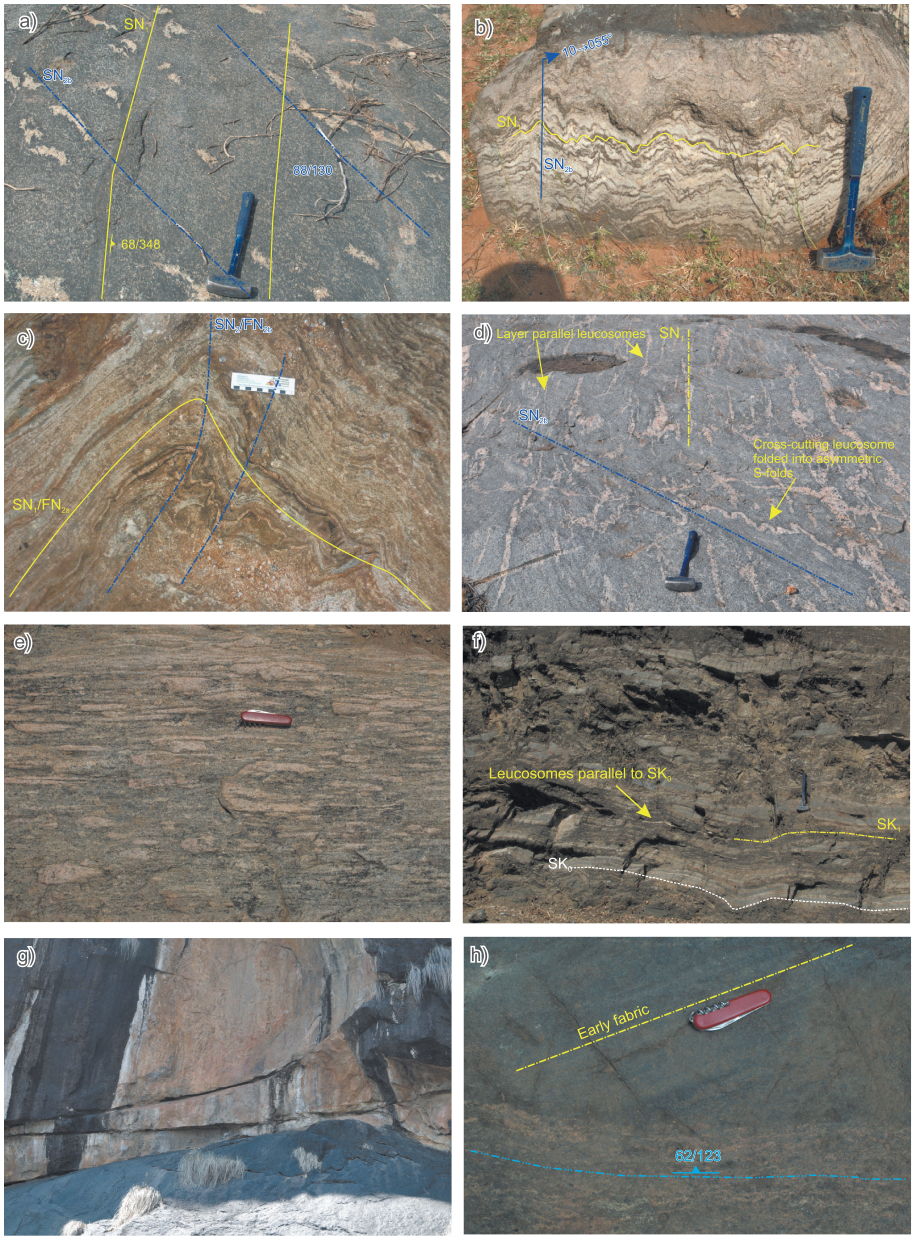

Figure 9. Field photographs depicting main structural features in the mapped transects of the Northern Madurai Block: (a) early amphibolite fabric (SN_1) crosscut by late NE-SW trending fabrics (SN_2) and dismembered plagioclase-quartz-rich leucosomes (NE Madurai Block transect); (b) calc-silicate metasedimentary rocks folded by NE-SW trending upright shallow plunging folds (FN_2, NE Madurai Block transect); (c) isoclinally folded (FN_1) calc-silicate metasedimentary rocks refolded by NE-SW trending FN_2 folds (NE Madurai Block transect); (d) primary NE-SW trending migmatitic fabrics (SN_1) within a granodioritic gneiss cut by late stage NNE-SSW trending fabrics (SN_2) both accompanied by in situ melt formation (NE Madurai Block transect); (e) highly strained augen gneisses with a well-developed L-tectonite fabric and shallow SW plunging mineral elongation lineations (NE Madurai Block transect); (f) migmatitic fabrics (SK_1) parallel to the sedimentary layering in the Kodaikanal Hills metasediments (Palni-Ganguvarpatti transect) (g) south dipping imbricate faults (DK_4) showing south side-up movements in the Kodaikanal Hills (Palni-Ganguvarpatti transect); and (h) early fabrics in mafic granulites cut by late stage granitic melts and SE dipping mylonitic foliations (SK_3, PGT transect).

the regional-scale calc-silicate unit (at the deflection point of the high-strain zone, Figure 8), porphyritic granitic gneisses are deformed into L-S tectonites (producing augen gneisses) that in places have a much better defined L-tectonite fabric characterized by preferential alignment of alkali feldspar aggregates and biotite (Figure 9e). The alkali feldspar phenocrysts form σ clasts showing a dextral sense of movement,

although in places the feldspar phenocrysts are symmetric (φ clasts) due to high strains associated with shearing. The mineral elongation lineation in the L-tectonites plunges gently (~10°) to the SW. This fabric is crosscut by late K-feldspar-plagioclase-quartz melt-dominated shears (~2–5 cm thick) trending NNE-SSW. Immediately south of the highly strained augen gneisses, muscovite-bearing quartzofeldspathic gneisses have subhorizontal dips and shallow SSW plunging lineations. At the southern margin of the transect, highly strained quartzite units form prominent circular ridges around a layered anorthosite-gabbro intrusion (Kadavur anorthosite, circa 829 Ma) [*Teale et al.*, 2011] with the structural fabrics suggesting they have a polydeformational history. The primary lithological layering (SN_0) is defined by the alignment of heavy mineral laminations and is visible in the thicker more competent layers in the lower strain domains. The earliest overprinting planar fabric (L-S tectonite, SN_1) is axial planar to meter scale isoclinal folds (FN_1) and parallel to the lithological (SN_0) layering. Sillimanite (later replaced by muscovite) and quartz minerals have a strong mineral preferred orientation parallel to this fabric, suggesting it was associated with higher temperatures of up to granulite-facies conditions. Outcrop-scale asymmetric Z folds with gentle SW plunges (10→240°) fold the SN_1 fabric and suggest NW side-up movement. However, they can also represent parasitic folds of the regional-scale NE-SW trending FN_2 folds recognized elsewhere. The extremely variable orientations of the $SN_{1/2}$ high-strain fabrics is due to the upright NNE-SSW trending open folds (FN_3) with moderately (~45–60°) south plunging fold axes. At outcrop scale, the intersection lineation between the fabrics produced quartz rods that are parallel to the FN_3 fold axes. The deformation during this stage was also accommodated by development of ESE dipping shear zones and moderately south plunging lineations that are subparallel to the axes of FN_3 folds. The latest deformation (DN_4) is associated with N dipping (~40–50°) reverse faults and development of E-W trending subvertical fracture cleavage observed at some outcrops. Shallow (~10°) west dipping normal faults most likely represent E-W extension associated with the N-S compression during this deformational phase.

Two samples (SI10-112 and SI10-113, Table 2) were dated to constrain the timing of the deformation. The sample SI10-113 is a granodioritic gneiss that intrudes the calc-silicate metasedimentary rocks. It preserves two phases of deformation (DN_1 and DN_2) and is crosscut by a late undeformed pegmatite (sample SI10-112). Zircon grains from sample SI10-113 show well-defined oscillatory-zoned cores surrounded by bright luminescent and dark luminescent sector-zoned rims under CL (Figure 5f). The U-Pb concordia plot of the granodioritic gneiss (SI10-113, Figure 6f) yielded upper and lower intercepts of 834 ± 34 Ma and 533 ± 97 Ma (MSWD = 1.6), respectively. The weighted average $^{206}Pb/^{238}U$ age of the concordant (≤5% discordant) analyses yielded an age of 789 ± 5 Ma (Figure 6f and Table 2), which is broadly consistent with the upper intercept age and is here interpreted as the age of crystallization of the granodioritic protolith. The lower intercept age (533 ± 97 Ma) is within error of a single concordant (0% discordant) age (541 ± 8 Ma) obtained from the moderately luminescent rim (Figure 5f, grain III). The low Th/U ratio (0.01), and the textural position of this analysis, suggests it is of metamorphic origin and is here interpreted as dating the age of metamorphism.

The U-Pb concordia plot for sample SI10-112 yields upper and lower intercepts of 810 ± 60 Ma and 497 ± 27 Ma, respectively (MSWD = 2.1, Figure 6g). The older zircon population came from the brightly luminescent oscillatory-zoned cores (Figure 5g) that yielded a weighted average $^{206}Pb/^{238}U$ age of 762 ± 7 Ma (MSWD = 1.2, Figure 6g) for the concordant (≤5% discordant) analyses. This upper intercept age is within error of the granodiorite crystallization age and most likely represents zircon inheritance from the granodiorite. A slight decrease in Th/U ratio with decrease in $^{206}Pb/^{238}U$ age (inset Figure 6) suggests that this old population may include zircon that has lost a minor amount of Th and Pb during subsequent Cambrian thermal perturbation. The zircon grains from sample SI10-112 show clear oscillatory-zoned overgrowths mantling the inherited zircon cores and yield a weighted mean $^{206}Pb/^{238}U$ age of 502 ± 4 Ma (MSWD = 1.8), which is within error of the lower intercept age. The nature of the overgrowths (oscillatory zoned, Figure 5g) and the high Th/U ratios (Figure 6) suggests growth from magma and is thus interpreted as dating the crystallization of the pegmatite.

4.3. Palni-Ganguvarpatti Transect

The Palni-Ganguvarpatti transect (PGT) extends for ~35 km in the NW-SE direction, crossing a major lithological and structural boundary between charnockite massifs (Palni and Kodaikanal Hills) to the west and the metasedimentary rock packages lying to the east (Figure 10). Field relationships between different lithological units are difficult to reconcile due to the dense rainforest. The best exposures were found in

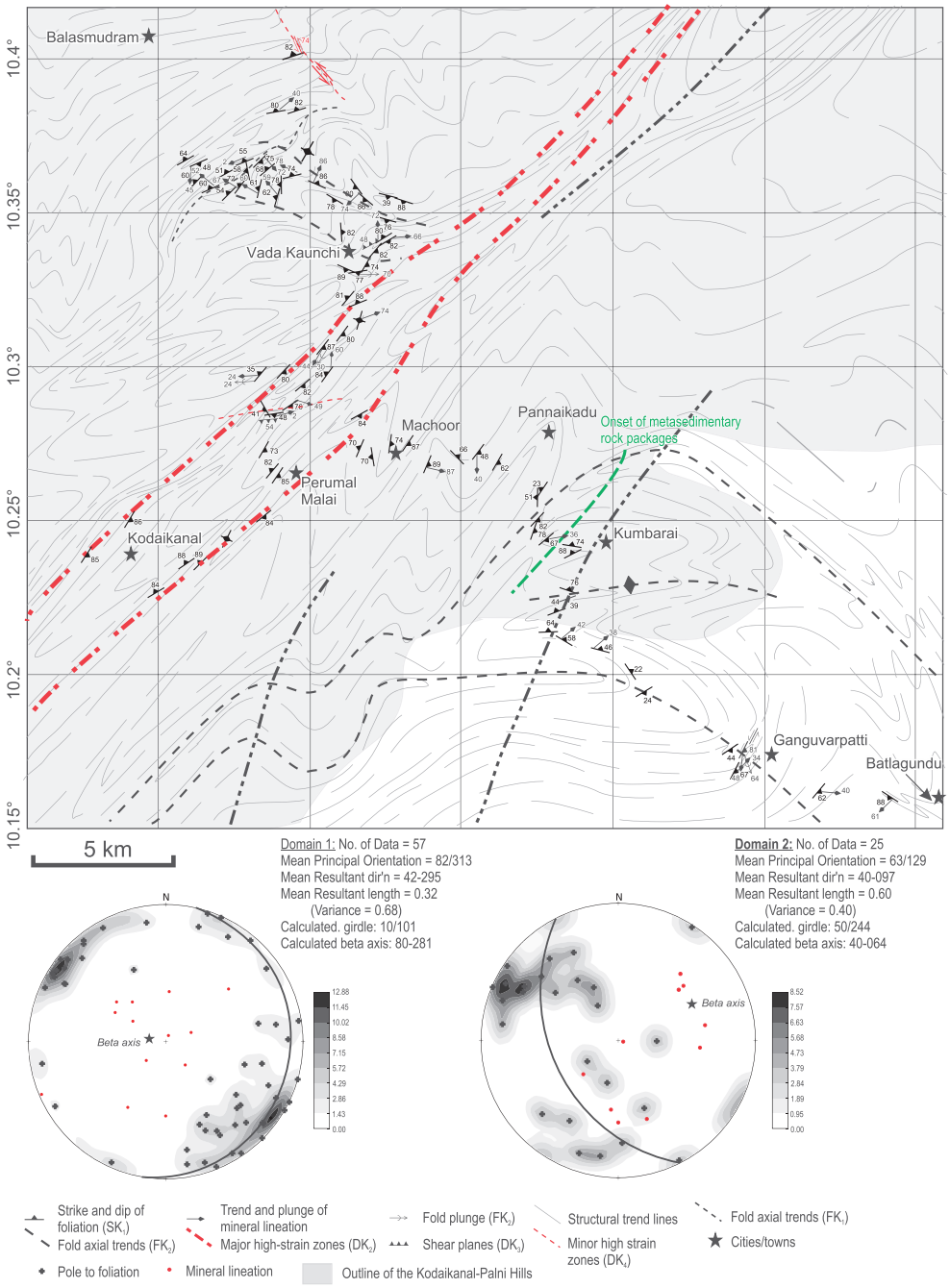

Figure 10. Structural map of the Palni-Ganguvarpatti transect and equal-area lower hemisphere stereographic projections for the measured structural components. Structural trends were defined through field observations coupled with satellite imagery. Domain 1—includes the NW part of the Palni-Ganguvarpatti transect between Balasmudram and Machoor. Domain 2—includes area to the SE of the Palni-Ganguvarpatti transect between Machoor and Batlagundu.

the road cuttings along the Palni-Kodaikanal-Batlagundu road. The transect was divided into two domains: Domain 1—charnockitic massifs of the Palni Hills area between Balasmudram and Perumal Malai and Domain 2—lower slopes of the Palni Hills massifs and predominantly flat-lying areas between Machoor and Batlagundu comprising largely metasedimentary lithologies. The boundary between the two domains is transitional and marked by a change in structural style and geometry as well as lithology. The relationship between the timing of deformational events (and their nomenclature) in the PGT transect with respect to the other structural transects is given in Table 4.

4.3.1. Domain 1—PGT

This domain is dominated by charnockitic (orthopyroxene-bearing felsic gneiss) lithologies interlayered with minor garnet-bearing metasedimentary rocks, hornblende-bearing gneisses, and amphibolites. A majority of the primary lithological relationships in this domain were obscured by later high-grade metamorphism. However, primary bedding (SK_0) of cm-scale interlayered psammitic and pelitic metasedimentary units shows them to be layer parallel to the migmatitic SK_1 fabric (Figure 9f). The earliest recognized high-grade event (DK_1) caused significant in situ partial melting of both igneous and sedimentary lithologies. Across the lithologies, the early high-strain planar fabric is characterized by alternating (1–10 cm thick) leucosomes with orthopyroxene-biotite-rich selvages and fine-grained mafic melanosome bands. Melanosomes are usually rich in biotite, hornblende, plagioclase, quartz, and minor orthopyroxene and clinopyroxene, while leucosomes are rich in alkali feldspar, quartz, and plagioclase but usually contain smaller proportions of mafic minerals (hornblende-orthopyroxene-biotite) as well as garnet in the more aluminous lithological units. On average, the foliations dip steeply to the NW and SE and have moderate to steep (~50–90°) variably plunging lineations (Figure 10). At one locality (10°20′15.7″N, 77°33′44.8″E), the SK_1 fabric is folded by steep rootless ESE plunging folds (FK_2, 73→122°). Within the migmatites, the mafic layers are often boudinaged layer parallel to the prominent planar fabric (SK_1) and surrounded by alkali feldspar dominated bands and leucosomes filling the boudin necks. Lower hemisphere equal-area projections (Figure 10) of the poles to foliation suggest that the interpreted regional-scale folds (FK_2) are steep to vertically plunging, similar to those observed at outcrop scale. Strongly foliated (73/315°) garnet-bearing leucosomes in more aluminous lithological units intrude along the axial planes of the regional FK_2 folds and have steep WNW plunging mineral lineations. The steep nature of the measured lineations that are broadly subparallel to the interpreted and observed fold axes (FK_2) suggest that this phase was associated with significant vertical extension. Coarse-grained orthopyroxene-bearing leucosomes and pegmatites often crosscut the main fabrics in a network pattern suggesting that partial melting continued under lower strains after the main fabric forming event (SK_1 or SK_2). South dipping (53/175°) cm thick biotite shear zones overprint and fold the high-strain fabrics within the metasedimentary sequences into E-W trending asymmetric north vergent reclined folds (FK_3) suggestive of south side-up movement. The mineral elongation lineations in the shear zone plunge shallowly (~19°) to the east and are parallel to the fold hinges of the reclined FK_3 folds. A subvertical E-W trending shape fabric (SK_4) overprints the FK_3 folds and is defined by an alignment of quartz crystals in the quartzites. A number of late brittle to brittle-ductile structures (DK_4) were observed. These include shallow south dipping imbricate thrusts (Figure 9g) suggesting south side-up movement and late stage mylonites (~1 m thick, 74/246° dip/dip direction) cutting across the charnockitic migmatites. The mylonite contains fragments of the country rock and quartz veins surrounded by tectonite fabrics, suggesting deformation took place under brittle-ductile conditions.

4.3.2. Domain 2—PGT

Domain 2 is dominated by metasedimentary sequences consisting of quartz-rich lithologies such as garnet-bearing psammites and quartzites, interlayered with cordierite-sillimanite-garnet-sapphirine-bearing migmatites and fine-grained hornblende-orthopyroxene-clinopyroxene-biotite-quartz amphibolites that usually occur as thick lenses and boudins within the metasedimentary lithologies. At the NW margin of Domain 2, between Perumal Malai and Machoor (Figure 10), well-foliated orthopyroxene-bearing felsic gneisses dip steeply to the WNW and become moderately E-SE dipping between Machoor and Pannaikadu (the transition zone). This zone is dominated by interlayered two-pyroxene and biotite-hornblende-bearing migmatitic gneisses with foliation dipping to the SE and NW. At one locality (10°16′10.3″N, 77°34′39.4″E), fine-grained mafic gneisses that preserve early NNW-SSE trending fabrics are intruded by granitic (alkali feldspar)-rich veins that have moderately SE dipping foliations (Figure 9h), suggesting that SE dipping planar fabrics are second generation fabrics (SK_2). The change in lithologies to predominantly metasedimentary rock units occurs directly west of Kumbarai (Figure 10). The contact between the metasedimentary rocks and the basement (foliated migmatitic two-pyroxene charnockite) was not observed in the field. However, near the contact with the metasedimentary rocks, the basement dips moderately to the SE, suggesting that it is structurally underlying the metasedimentary rocks farther east. The metasedimentary rock packages near the contact with the basement dip steeply to the NNW-NNE and SSE. Garnet-biotite-bearing migmatites near the contact are characterized by well-defined planar fabrics (SK_1), layer-parallel leucosomes, and thick bands of quartz and biotite-rich domains (psammitic layers) that contain minor orthopyroxene. The

metasedimentary rocks farther SE along the Kumbarai-Ganguvarpatti road become progressively more politic, characterized by appearance of cordierite-, sapphirine-, and sillimanite-bearing assemblages, lower proportions of quartz, and higher proportion of alkali feldspar-rich leucosomes that are commonly folded axial planar to the pervasive NNE dipping migmatitic fabric (SK_2). Mineral elongation lineations, defined mostly by biotite and quartz minerals, plunge moderately (~40°) to the NE. Midway between Kumbarai and Ganguvarpatti, the foliation changes from predominantly NNE dipping to moderately SE dipping thus defining regional-scale FK_3 folds with interpreted ENE plunging fold axes (Figure 10). Near Ganguvarpatti, garnet-biotite-bearing migmatitic gneiss lies structurally above two-pyroxene felsic gneiss and is overlain by a thick (~20 m) quartzite unit. The migmatitic foliation in the two-pyroxene felsic gneiss is cut by shallow SE dipping shear zones that fold the early fabric (SK_1) in the charnockite producing macroscale recumbent Z folds looking toward the SE. These shears are later crosscut by pyroxene and hornblende-bearing pegmatites. Garnet-bearing leucosomes in the garnet-biotite-bearing gneiss are isoclinally folded with steeply SSE plunging fold axes and subparallel mineral elongation lineations. The lineations in the overlying quartzites are defined by the stretched quartz grains and are subparallel to the axes of the regional NE plunging FK_3 folds. Regional structural trends reveal kilometer scale NNE-SSW trending open folds (FK_4) that fold the axial planes of the mesoscale FK_3 folds. At one locality (10°13′45.5″N, 77°38′18.8″E), subvertical ~N-S trending fracture cleavage overprinting the migmatitc fabric in garnet-biotite-bearing gneisses most likely represents deformation during the late stage FK_4 folding. Late undeformed orthopyroxene-hornblende-bearing pegmatites that commonly crosscut the orthogneisses are not commonly found cutting across the metasedimentary sequences. No geochronological study was carried out for this transect due extensive geochronological data already made available by previous studies (see Figure 11).

5. Discussion

5.1. Structural Evolution and Timing of Deformation

The time-space plot in Figure 11 summarizes the relative timing of the observed structural fabrics from across the three transects. The discussion below presents the interpreted scenario regarding the timing and relationships between different structural fabrics from across the Salem and Madurai Blocks (see Table 4) based on field observations and U-Pb zircon geochronology of crosscutting features.

5.1.1. PCSS

A total of five deformational events (DP_1–DP_5) can be recognized within this transect, with the timing and the style of the deformation varying between the four domains recognized within the PCSS transect. The summary of the timing and the style of the main deformational events are given in Table 3. Domains 1 and 2 of the PCSS transect share a common deformational history with the development of early gneissic migmatitic fabrics (SP_1) in which garnet-clinopyroxene-plagioclase mafic assemblages are stable. The original orientation of the SP_1 gneissic fabrics are overprinted by heterogeneously distributed DP_2 strain. The DP_2 strain in the Moyar-Salem-Attur shear zone (Domain 1—PCSS transect) is associated with development of a high-strain dextral strike-slip mylonites. Immediately south of the Moyar-Salem-Attur shear zone (within Domain 2), DP_2 strain is characterized by high-grade amphibolite to granulite-facies deformation during NW block-up movement as characterized by cm-scale NW dipping dextral shears and regional-scale FP_2 folds all intruded by granitic melts. The strain partitioning during DP_2 deformation between the high-strain Moyar-Salem-Attur shear zone and fold-dominated low-strain domains (Domain 2—PCSS transect) has most likely developed during bulk NW-SE shortening and corresponding E-NE extension defined by mineral stretching lineations. Biotite rims around rotating garnets during DP_2 strain (Domain 1) and retrogression to predominantly hornblende-bearing and biotite-bearing assemblages of rocks farther south suggest that DP_2 phase was associated with decompression during NW-SE shortening.

The timing of the high-grade event DP_1 associated with development of garnet-clinopyroxene-plagioclase mafic assemblages and migmatization was constrained to circa 2510–2480 Ma based on zircon and monazite U-Pb geochronology of the Kanja Malai mafic granulites [*Saitoh et al.*, 2011; *Sato et al.*, 2011b; *Anderson et al.*, 2012] as well as garnet Lu-Hf isochron ages [*Noack et al.*, 2013] within Domain 1 and metamorphic zircon ages of Archean granodiorite gneisses within Domain 2 farther south (sample SI10-24 this study, Figure 11 and Table 2). Conventional thermobarometry and P-T pseudosection calculations on

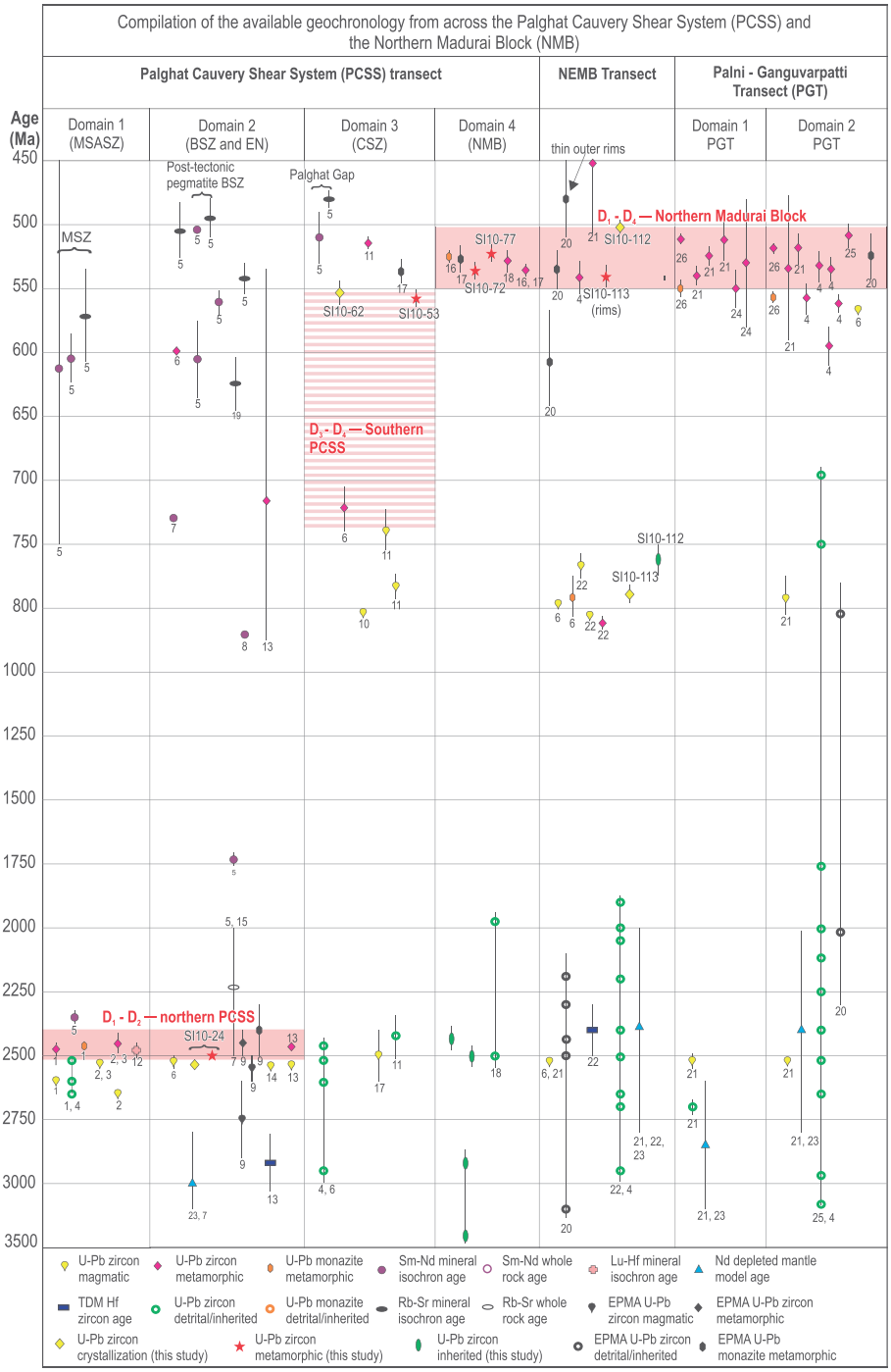

Figure 11. Time-space plot of the compiled geochronological data from across the Palghat-Cauvery Shear System (PCSS) and the Northern Madurai Block (NMB). The areas shaded in red represent major metamorphic and deformational events within the Southern Granulite Terrane. Geochronological references used are as follows: (1) *Anderson et al.* [2012], (2) *Sato et al.* [2011b], (3) *Saitoh et al.* [2011], (4) *Plavsa et al.* [2014], (5) *Meißner et al.* [2002], (6) *Ghosh et al.* [2004], (7) *Bhaskar Rao et al.* [1996], (8) *Bhutani et al.* [2007], (9) *Santosh et al.* [2003], (10) *Sato et al.* [2011a], (11) *Santosh et al.* [2012], (12) *Noack et al.* [2013], (13) *Mohan et al.* [2013], (14) *Yellappa et al.* [2012], (15) *Raith et al.* [1999], (16) *Clark et al.* [2009a], (17) *Collins et al.* [2007a], (18) *Raith et al.* [2010], (19) *Rao et al.* [1994], (20) *Santosh et al.* [2006], (21) *Plavsa et al.* [2012], (22) *Teale et al.* [2011], (23) *Tomson et al.* [2013], (24) *Prakash et al.* [2010], (25) *Collins et al.* [2007b], and (26) *Clark et al.* [2014].

AGU Tectonics

10.1002/2014TC003706

Table 3. Deformational Events Along the Palghat-Cauvery Shear System (PCSS) Transect

	Domain 1	Domain 2	Domain 3	Domain 4
D_1 Circa 2.5–2.49 Ga	Early gneissic migmatitic fabrics (SP_1) isoclinally folded. Fabrics are mostly preserved within the lower strain zones. Granulite-facies conditions	Early gneissic migmatitic fabrics (SP_1) variably folded by regional-scale NE-SW trending folds Granulite-facies conditions	No pre-D_3 structures observed	No pre-D_4 structures observed
D_2 Circa 2.49–2.45 Ga	High-strain L-S mylonitic (SP_2) fabrics parallel to the axial planes of the isoclinal folds with moderately east plunging fold axes Noncoaxial dextral strike-slip shearing, with minor component of vertical movement	Folding of early gneissic fabric by NE-SW trending regional-scale folds (FP_2) with shallow doubly plunging fold axes and subparallel mineral elongation lineations Development of NW dipping cm-scale shear bands Amphibolite-facies conditions NW-SE noncoaxial shortening	No pre-D_3 structures observed	No pre-D_4 structures observed
Igneous activity (circa 820–740 Ma)			Mafic intrusions in a suprasubduction-type setting (Manamedu Complex)	
D_{3a} Circa 0.74–0.55 Ga	Large-scale WSW-ENE folds (FP_3) with steep NW plunging fold axes Quartz ridges form parallel to the axial planes of FP_3 folds	Deformation associated with development of SSE dipping shear zones Folding of the $SP_{1/2}$ fabrics by upright moderately SE plunging folds (FP_3) Amphibolite-facies?	High-grade gneissic fabrics (SP_{3a}) and development of thin (1–2 cm) garnet-clinopyroxene-plagioclase and slightly thicker (up to 5 cm) clinopyroxene-plagioclase-quartz gneissic bands Granulite-facies conditions	No pre-D_4 structures observed
D_{3b} Circa 0.74–0.55 Ga	No post-D_3 structures observed	No post-D_4 structures observed	Lower strain domains: shape fabric (SP_{3b}) parallel to the axial planes of the ESE-WSW trending FP_{3b} folds High-strain zones: ~400 m wide mylonitic north dipping shear zone (SP_{3b}) and moderately north dipping mineral elongation lineations North side-up movement that is largely dip slip, with only a minor component of dextral strike-slip movement Upper amphibolite-facies? Dextral transpression	No pre-D_4 structures observed
D_4 Circa 0.74–0.55 Ga	No post-D_3 structures observed	Shallow south dipping shear zones with gently east plunging mineral lineations	Development of large-scale, shallow north dipping shear zones and recumbent folds (FP_4) with attenuated lower	Development of early migmatitic fabric (SP_4) characterized by alternating leucosome (kfs-pl-qtz) and mesosome (gt-hbl-bt-qtz)

AGU Tectonics

10.1002/2014TC003706

Table 3. (continued)

	Domain 1	Domain 2	Domain 3	Domain 4
			limbs with north side-up movements	bands several centimeters thick
		Amphibolite-facies. Significant retrogression of opx-cpx mafic assemblages. Intrusion of alkaline complexes (Sankaridurg granite U-Pb zircon age of 556 ± 3 Ma [*Brandt et al.*, 2014]; Sivamalai Alkaline Complex, Rb-Sr WR isochron age of 623 ± 21 Ma [*Rao et al.*, 1994]) Possible south side-up movement	Amphibolite-facies retrogression and intrusion of pegmatites (circa 550 Ma dated in this study)	Granulite-facies conditions
Undeformed pegmatite (circa 550 Ma)			Pegmatite intrusion, sample SI10-62 (554 ± 9 Ma)	Crosscutting granitic vein, sample SI10-53 (556 ± 14 Ma)
D_{5a} Circa 0.55–0.52 Ga	No post-D_4 structures observed	No post-D_4 structures observed	No post-D_4 structures observed	Isoclinal folding of the migmatitic fabric (SP_4) and development of predominant L-S fabric (SP_{5a}) axial planar to the isoclinal folds (FP_{5a}) Leucosome age (sample SI10-72, 538 ± 7 Ma) Granulite- to amphibolite-facies conditions
D_{5b} Circa 0.53–0.52 Ga	No post-D_4 structures observed	No post-D_4 structures observed	No post-D_4 structures observed	Development of NNE-SSW trending folds (FP_{5b}) with moderate to steeply NNE plunging fold axes and subparallel mineral elongation lineations Development of cm-scale NW dipping sinistral (in the horizontal plane) ductile shear bands Amphibolite-facies conditions
Undeformed pegmatite (circa 520 Ma)				Undeformed pegmatite cutting across all of the fabrics (sample SI10-77, 523 ± 6 Ma)

Table 4. Summary of the Main Deformational Events and Their Nomenclature Between the Three Structural Transects

	Salem Block		Cauvery Shear Zone	Madurai Block		
Timing of Deformational Events	Domain 1-PCSS Transect	Domain 2-PCSS Transect	Domain 3-PCSS Transect	Domain 4-PCSS Transect	NEMB Transect	PGT Transect
Circa 2.5–2.45 Ga	DP_1 and DP_2	DP_1 and DP_2	None known	None known	None known	None known
Circa 0.74–0.55 Ga	DP_3	DP_3	DP_3 and DP_4	DP_4	DN_1	DK_1
Circa 0.55–0.50 Ga	None known	None known	None known	DP_{5a}, DP_{5b} and DP_6	DN_2 and DN_3	DK_2 and DK_3
Circa $<$ 0.50 Ga	None known	None known	None known	None known	DN_4	DK_4 and DK_5

the garnet-bearing mafic granulites, charnockites, and garnet-kyanite-bearing paragneisses from the Kanja Malai locality yielded pressures of up to 16 kbar and temperatures between ~820 and 860°C [*Saitoh et al*., 2011; *Sato et al*., 2011b; *Anderson et al*., 2012; *Noack et al*., 2013]. The best estimate for the timing of DP_2 deformational event can be loosely constrained to between circa 2480 Ma and circa 800 Ma (intrusion of Manamedu ultramafic complex farther south) [*Santosh et al*., 2012]. However, somewhat younger (2467 ± 10 Ma) [*Anderson et al*., 2012] U-Pb monazite ages obtained from garnet-kyanite-bearing paragneisses at Kanja Malai could indicate decompression during DP_2 uplift through U-Pb-Th diffusion closure temperatures in monazites, which in relatively dry metamorphic conditions can exceed 750–800°C [*Rubatto et al*., 2001].

The extent of the widespread high-grade Paleoproterozoic event (DP_1) is also evident toward the west where U-Pb zircon ages of Sittampundi anorthosite yielded Neoarchean crystallization ages (2541 ± 13 Ma) and Paleoproterozoic (2461 ± 15 Ma) metamorphic ages [*Mohan et al*., 2013]. However, the analyzed zircons at the Sittampundi anorthosite also show Pb loss at 715 ± 180 Ma [*Mohan et al*., 2013] from some of the metamorphic zircons, which is in agreement with circa 726 Ma garnet-clinopyroxene-plagioclase-whole rock (WR) Sm-Nd isochron age obtained from the mafic granulites at the same locality [*Bhaskar Rao et al*., 1996].

Toward the southern margin of the PCSS transect, and consequently the Salem Block, the $SP_{1/2}$ fabrics are overprinted by DP_3 strain which is associated with development of the high-strain Cauvery shear zone (CSZ—Domain 3) as well as lower strain SSE dipping shear zones immediately to the north of the CSZ. The early gneissic fabrics in Domain 3 (SP_{3a}—Cauvery shear zone) are characterized by significant differentiation of garnet-clinopyroxene- and clinopyroxene-orthopyroxene-rich restites and clinopyroxene-plagioclase-quartz-rich leucosomes during high-grade metamorphism. It should be noted that the timing of the high-grade metamorphism and differentiation within the shear zone itself is poorly constrained and not likely to be coeval with the high-grade metamorphism farther north. One line of evidence supporting this statement is the similarity of structural and geometric styles of the SP_{3b} fabrics in Domains 2 and 3, which overprint the earlier $S_{1/2}$ fabrics farther north. U-Pb dating of zircons from a mafic granulite within the Cauvery shear zone farther east, along strike, yielded circa 2.5 Ga and circa 2.9 Ga ages from rims and cores of the zircon grains, respectively, and a younger concordant zircon population at 722 ± 13 Ma [*Ghosh et al*., 2004] obtained from anhedral zircons in the same sample (location 6, Figure 2). The younger, early Neoproterozoic, age is comparable to the garnet-clinopyroxene-plagioclase-WR Sm-Nd isochron age of the Sittampundi mafic granulites farther west [*Bhaskar Rao et al*., 1996] and circa 740 Ma U-Pb zircon crystallization age for deformed plagiogranite- and gabbro-layered mafic-ultramafic complex (Manamedu Ophiolite) farther east within the Cauvery shear zone [*Santosh et al*., 2012]. For this reason, the best lower estimate for the formation of the SP_3 fabrics (collectively SP_{3a} and SP_{3b}) within Domain 3 is taken as circa 800–720 Ma. The dominant mylonitic fabrics (DP_{3b} of the PCSS transect) in the Cauvery shear zone dip to the north and are associated with north block-up movements under higher-grade conditions as confirmed by the stability of plagioclase and clinopyroxene in the mylonitic fabric and the presence of tonalitic melts. The WNW-ESE high-strain mylonites and corresponding north plunging mineral elongation lineations suggest north block-up movements in a dextral transpressive stress regime during bulk ~N-S shortening. In lower strain, fold-dominated, domains, this deformational phase is also associated with extension parallel to WNW-ESE trending doubly plunging folds.

The latest deformational phase (DP_4) has affected both Domains 2 and 3. To the north and within the Cauvery shear zone, this phase is associated with development of shallow south and north dipping amphibolite-facies shear zones that resulted in retrogression of the mafic granulites to hornblende-plagioclase-bearing mineral assemblages. Along the DP_4 shear zones, numerous undeformed (circa 554 Ma, sample SI10-62) pegmatites intrude into garnet-clinopyroxene-plagioclase-quartz mafic granulites providing the upper limit for the DP_3 deformation and the lower limit for the DP_4 deformation. This age is similar to the age of crosscutting granitic vein (sample SI10-53, 556 ± 14 Ma) immediately to the south of the Cauvery shear zone. The structural character of the DP_4 shear zones suggests that they are associated with amphibolite-facies (middle crustal) deformation and significant vertical shortening and lateral extension quite possibly associated with postcollisional collapse due to overthickened crust.

Domain 4 of the PCSS transect is somewhat different in structural character and relative timing of deformational events. The earliest high-grade fabrics are associated with significant in situ partial melting and migmatization (DP_4) of Archean igneous and sedimentary protoliths (see Tables 2 and 4). The age of melting and migmatization was obtained from U-Pb dating of recrystallized zircon grains [*Hoskin and Black*, 2000] and sector-zoned overgrowths (sample SI10-72) typically associated with growth during anatexis [*Vavra et al*., 1996]. The upper limit for DP_4 migmatization event is therefore constrained to 556–538 Ma (Table 2). The leucosomes are isoclinally folded, and the resulting overprinting axial planar fabrics (DP_{5a}) form the predominant structural grain in this domain. The second generation fabrics (SP_{5b}) in this domain are overprinted by regional and outcrop-scale NNE plunging folds (DP_6). A late crosscutting pegmatite dated at 523 ± 6 Ma gives an upper estimate for the deformation in this domain. The age of high-grade metamorphism associated with migmatization (DP_4) and postmigmatization deformation ($D_{5a/b}$) is therefore loosely constrained between 556 and 523 Ma. High-precision SHRIMP U-Pb geochronology of metamorphic zircons (including overgrowths) and monazites from the garnet-kyanite-biotite gneiss at the Panangad locality (locality 7, Figure 2) yielded similar ages of circa 535 Ma and circa 525 Ma, respectively [*Collins et al*., 2007a; *Clark et al*., 2009a]. Furthermore, less precise electron probe micro-analyzer (EPMA) monazite ages from corundum- and sapphirine-bearing granulite-facies rocks within this domain also yielded late Neoproterozoic metamorphic ages (550–520 Ma) [*Santosh et al*., 2006] giving further evidence of a pervasive late Neoproterozoic high-grade event. The P-T-t modeling from the Panangad locality [*Clark et al*., 2009a] suggests migmatization occurred at temperatures of 670–724°C and pressures of up to 8 kbar followed by crustal thickening during north block-up movement and finally by reheating and decompression during slab delamination.

5.1.2. North Eastern Madurai Block Transect

Four deformational events (D_1–D_4) have been identified in the NE Madurai Block. The earliest high-strain fabrics (DN_1) recognized in the igneous gneisses are associated with migmatization as well as subvertical NNW dips similar to the rocks of Domain 4 within the PCSS transect (DP_4—directly south of the Cauvery shear zone). The earliest fabrics (DN_1) in the metasedimentary rocks farther south (calc silicates and quartzites), however, are concordant to the primary lithological layering (SN_0) and axial planar to isoclinal FN_1 folds. The character of the FN_1 folds in the metasedimentary rocks is difficult to unravel due to later deformation and refolding ($FN_{2/3}$), and it is therefore difficult to say with any certainty whether the SN_1 fabrics in metasedimentary rocks and migmatitic gneisses farther north are coeval. South of this transect, *Drury et al*. [1984] and *Srinivasan and Rajeshdurai* [2010] reported kilometer scale early recumbent folds (FN_1) within the metasedimentary sequences that are likely to reflect the earliest phase of deformation in the Northern Madurai Block (DN_1). The early recumbent folds (FN_1) are overprinted by second generation fabrics during DN_2 and are responsible for the regional-scale structural patterns producing outcrop and regional-scale NE-SW trending folds with doubly plunging fold axes. The high-strain Muthampatti-Palayam-Eriyody (MPE) shear zone is characterized by porphyritic K-feldspar augen gneisses (in places forming L-tectonites) that have moderately SE dipping fabrics and shallow SW plunging lineations. Shallow plunging lineations parallel to the fold axes of F_2 folds and the associated high-strain MPE shear zone suggest the presence of a significant component of vertical shortening and subhorizontal extension, possibly, during postorogenic collapse. The high-strain fabrics within the MPE shear zone are crosscut by cm-scale melt-induced sinistral shears that typically have NNE-SSW trends. The late NNW-SSE trending fabrics associated with cm-scale sinistral shears and asymmetric FN_3 folds between the shear bands are common north and south of the MPE shear zone. Similarly, oriented upright folds with SSW plunging axes

and NNE-SSW shear zones deform the early high-strain fabrics ($SN_{1/2}$) in quartzites. It is difficult to say with any certainty whether NE-SW (SN_2) and NNE-SSW (SN_3) fabrics represent separate events or whether they formed contemporaneously. Late upper crustal deformation is characterized by north dipping reverse thrusts, E-W trending fracture cleavages and west dipping extensional faults (collectively DN_4) all interpreted to reflect upper crustal deformation during N-S directed shortening.

The early migmatitic fabric within the early Neoproterozoic (circa 790 Ma) granodioritic gneiss intrusive into the calc-silicate rocks most likely represents the metamorphic overprint during DN_1 (circa 541 Ma). Although there are reports of an earlier metamorphic overprint (circa 800–750 Ma) determined from the U-Pb dating of zircon rims in metasedimentary rocks [*Teale et al*., 2011; *Plavsa et al*., 2014], we interpret these ages represent contact metamorphism resulting from large volumes of Cryogenian magmatic intrusions above the interpreted coeval subduction zone [*Tomson et al*., 2006; *Santosh et al*., 2012]. The age of metamorphism associated with migmatization is similar to the ages (556–538 Ma) of migmatitic leucosomes obtained farther north within Domain 4 (PCSS transect). The upper limit of the second generation fabrics (DN_2) in the gneiss is given by the age of the late undeformed pegmatite (502 ± 4 Ma, SI10-112). It is difficult to say with any certainty whether DN_2 and DN_3 deformational events were coeval. The latest deformational event (DN_4) associated with N-S shortening may correlate with late Neoproterozoic (circa 530–480 Ma) [*Ghosh et al*., 2004] south block-up movement along the Achankovil shear zone farther south [*Cenki and Kriegsman*, 2005].

5.1.3. Palni-Ganguvarpatti Transect

The metaigneous and metasedimentary rocks from across the KKPT shear zone (Domains 1 and 2) have common deformational histories with five (D_1–D_5) deformational phases recognized (Table 4). The earliest phase was associated with significant melting of both Archean orthogneiss protoliths to the west and Archean to early Neoproterozoic metasedimentary rocks to the east. During this phase (DK_1), significant in situ partial melting and boudinage of the mafic rocks took place. The early DK_1 migmatitic fabrics are layer parallel to the sedimentary layering in the metasedimentary rock packages (Figure 8g) and most likely represent melting due to crustal thickening and heating. The rocks were then exhumed during NW-SE directed horizontal shortening (DK_2) as characterized by steep to subvertical mineral stretching lineations, tight to isoclinal subvertically plunging folds that are evident in both domains of the PGT transect. The original azimuths of the DK_2 mineral stretching lineations are more difficult constrain in the metasedimentary rocks of the Domain 2 due to later overprinting fabrics ($DK_{3/4}$). Strain partitioning between the metasedimentary rocks to the east (open upright NE-SW trending folds with NE plunging fold axes and parallel mineral elongation lineations) and charnockitic massifs to the west (biotite-rich SSE dipping shear zones) occurs during the DK_3 deformational event. Post-DK_3 deformational phases are somewhat less well-characterized particularly since late stage (DK_4) deformation inferred from the regional-scale trends and variations in the orientation of foliations is only evident in the eastern metasedimentary-dominated areas (Domain 2). Upper crustal deformation (DK_5) is characterized by SSW dipping imbricate thrusts, subvertical E-W trending shape fabrics, and NW-SE trending mylonitic shear zones all indicate deformation during bulk ~N-S shortening. Late orthopyroxene-bearing leucosomes cut the early DK_1–DK_3 fabrics, but their relationship with DK_4 and DK_5 deformation is uncertain. The orthopyroxene-bearing leucosomes commonly form veined networks and appear undeformed at outcrop scale and may indicate intrusion during postcollisional orogenic collapse.

The timing of the high-grade metamorphism (DK_1) is best constrained by U-Pb zircon dating of leucosomes in the western part of the Palni-Ganguvarpatti transect that yielded an age of 554 ± 5 Ma [*Brandt et al*., 2011]. This age is in very good agreement with the ages (560–520 Ma) obtained from U-Pb dating of monazites and metamorphic zircons in charnockitic and metasedimentary protoliths [*Santosh et al*., 2003, 2006; *Brandt et al*., 2011; *Plavsa et al*., 2012, 2014; *Clark et al*., 2014], as well as migmatitic layers farther north (this study). Some authors [*Raith et al*., 1997; *Brandt et al*., 2011] suggest the possibility of an early Proterozoic (circa 2.45 Ga) metamorphism affecting the Northern Madurai Block protoliths based on zircon evaporation ^{207}Pb-^{206}Pb dating of Kodaikanal Hills charnockites [*Bartlett et al*., 1998] and LA-ICP-MS U-Pb zircon dating of inherited cores in restitic granulites [*Brandt et al*., 2011]. However, we believe this is not likely as the early Proterozoic ages obtained by zircon evaporation methods of *Bartlett et al*. [1998] suggest crystallization rather than metamorphic ages (oscillatory-zoned zircon cores) and the ambiguous textural interpretations

of small dark unzoned cores as well as high Th/U ratios of zircon cores obtained by *Brandt et al*. [2011] most likely suggest the ages represent crystallization ages of the protoliths (igneous or sedimentary). The strong planar fabrics and subvertical extension lineations found in both domains (DK_2) most likely represent the exhumation of the terrane during the retrograde stage of the P-T evolution associated with decompression. The high proportion of undeformed leucosomes concordant to DK_2 fabrics suggests high-temperature melt-dominated conditions during exhumation. The stability of biotite and hornblende in DK_2 fabrics most likely represents cooling of the terrane at midcrustal levels (5–7 kbar) and equilibration of high-grade assemblages through back reactions with the crystallizing melt [*Raith et al*., 1997; *Sajeev et al*., 2006; *Brandt et al*., 2011; *Clark et al*., 2014]. Recently, *Clark et al*. [2014] obtained SHRIMP U-Pb ages of circa 518–508 Ma for high-Y monazites and zircon rims in metapelites from Kodaikanal Hills. The textural position of zircon grains (within cordierite coronas around garnet and within late biotite), along with the geochemistry of monazite (high Y), is consistent with growth during breakdown of garnet and growth of zircon during crystallization of melt [*Kelsey et al*., 2008; *Clark et al*., 2014]. For this reason, the DK_2 event is poorly constrained between 550 Ma and 500 Ma. The circa 485 Ma Rb-Sr ages of biotites from retrogressed granulites in the Anaimalai Hills farther west in this transect are in broad agreement with continued exhumation of the terrane at this time. The lower limit for the DK_3 deformation can be broadly correlated with the upper limit of the DK_2 deformation at 550–485 Ma. Post-DK_3 deformational events (DK_4–DK_5) are difficult to constrain due to lower temperature upper crustal nature of the deformation, and as such, other methods such as lower temperature thermochronology (zircon and apatite fission track and ^{40}Ar-^{39}Ar muscovite dating) are more applicable and warrant further investigation.

5.2. Structural and Tectonic Evolution of the Southern Granulite Terrane

The structural evolution of the Southern Granulite Terrane differs from north to south across the Palghat-Cauvery Shear System and into the Northern Madurai Block. The earliest deformational event (DP_1/DP_2) associated with high-pressure-high-temperature (HP-HT) metamorphism at the northern margin of the Palghat-Cauvery Shear System (the Moyar-Salem-Attur shear zone) is constrained to circa 2.5–2.45 Ga, which is considerably older than the age of the high-grade fabrics at the southern margin of the shear system (the Cauvery shear zone) that is interpreted to have formed in the Neoproterozoic (Figure 11). The Early Paleoproterozoic metamorphic event is prevalent throughout the Eastern Dharwar Craton, where it reworks juvenile Neoarchean (circa 2.7–2.5 Ga) to Mesoarchean (eastern margins of the Western Dharwar Craton) rocks and is attributed to subduction-accretion tectonics along the eastern margin of the Western Dharwar Craton [*Anderson et al*., 2012; *Peucat et al*., 2013; *Glorie et al*., 2014]. The Moyar-Salem-Attur shear zone is believed to be responsible for juxtaposing the relatively juvenile Neoarchean Nilgiri massif (circa 2.5–2.7 Ga) [*Bhaskar Rao et al*., 2003; *Tomson et al*., 2006; *Peucat et al*., 2013; *Santosh et al*., 2015] against granite-greenstone belts of the Western Dharwar Craton during dextral strike-slip motion with inferred offsets in the range of 80–120 km based on satellite imagery and crustal evolution similarities to those of Madras massifs in the easternmost parts of the Southern Granulite Terrane [*Drury et al*., 1984; *Peucat et al*., 2013]. Early Paleoproterozoic metamorphic overprints are evident as far south as locality 6 (Figure 2), although the highly discordant nature of the analyses and significant Pb loss during the Neoproterozoic metamorphism complicates the interpretation [*Ghosh et al*., 2004]. Late Neoproterozoic (circa 620–550 Ma) deformation at the northern margin of the Palghat-Cauvery Shear System is restricted to narrow shear zones that cause significant retrogression of high-grade rocks to biotite-bearing assemblages [*Raith et al*., 1999; *Meißner et al*., 2002], suggesting reactivation of Paleoproterozoic high-strain shear zones during the Neoproterozoic. The high-strain fabrics within the Cauvery shear zone ($DP_{3a/3b}$ of Domain 3) formed prior to the intrusion of pegmatites at circa 550 Ma. The complexities associated with using zircon geochronology to date the high-strain fabrics ($SP_{3a/3b}$) within the shear zone are illustrated by *Plavsa et al*. [2014] where multiple thin zircon overgrowths are evident. However, the highly strained early Neoproterozoic (circa 820–740 Ma) mafic-ultramafic complex (Manamedu Ophiolite Complex) [*Sato et al*., 2011a; *Santosh et al*., 2012] within the Cauvery shear zone provides a lower estimate for the deformational event associated with the high-grade ~E-W trending fabrics of the Cauvery shear zone. Consequently, peak metamorphic gneissic fabrics along with the overprinting high-strain fabrics (DP_{3a} and DP_{3b}) of the Cauvery shear zone are broadly constrained to have occurred sometime between circa 740–550 Ma. Although both the Cauvery and Moyar-Salem-Attur shear zones preserve granulite-facies assemblages

(garnet-clinopyroxene-plagioclase-quartz mafic granulites), the disparity in their structural characteristics (predominantly dextral noncoaxial strain with east plunging lineations in the Moyar-Salem-Attur shear zone, compared to dip-slip deformation with a minor component of dextral strike-slip movement during bulk ~N-S shortening of the Cauvery shear zone) and age constraints (early Paleoproterozoic versus Neoproterozoic) demonstrates that they are not contemporaneous. The complex folding patterns between the two major shear zones (Figure 2) are a product of multiple deformational events spanning the early Paleoproterozoic to the late Neoproterozoic. As a result, interpreting the Palghat-Cauvery Shear System as a set of anastomosing Neoproterozoic shear zones with overall dextral shear sense [*Drury et al*., 1984; *Chetty and Bhaskar Rao*, 2006b, 2006c] appears an oversimplification.

Immediately south of the Cauvery shear zone, within the Northern Madurai Block, the earliest fabrics are associated with high-pressure-ultrahigh temperature (HP-UHT) metamorphism (up to 15 kbar and 950–1150°C) [*Collins et al*., 2014a, and references therein], during which significant in situ partial melting of Archean to Neoproterozoic igneous to sedimentary protoliths occurred [*Santosh et al*., 2006; *Collins et al*., 2007a; *Collins et al*., 2007b; *Teale et al*., 2011; *Plavsa et al*., 2012, 2014]. The best constraints on the timing of this event (D_1—collectively made up of DN_1 and DK_1 of NEMB and PGT transects, respectively) were provided by leucosome U-Pb zircon dating that yielded ages of circa 556–538 Ma (this study) and is in agreement with the 554 ± 5 Ma age of leucosomes in the Kodaikanal Hills [*Brandt et al*., 2011], as well as peak metamorphic ages obtained from SHRIMP U-Pb dating of low-Y monazites (suggestive of growth in equilibrium with garnet) in Kodaikanal Hills metapelites at 559 ± 4 Ma [*Clark et al*., 2014]. Phase equilibria modeling of metasedimentary rocks in close proximity to the Cauvery shear zone yielded pressures of up to 15 kbar [*Collins et al*., 2014a] and up to 12–13 kbar farther south in the PGT transect [*Raith et al*., 1997; *Sajeev et al*., 2004, 2006]. Ultrahigh-temperature (UHT) metamorphic conditions (up to 1100°C) were attained subsequent or contemporaneous with HP metamorphism in the Northern Madurai Block [*Raith et al*., 1997; *Clark et al*., 2009a; *Brandt et al*., 2011; *Clark et al*., 2014] giving rise to a clockwise P-T path. In addition, *Clark et al*. [2009a] suggest a more complex P-T-t evolution for rocks in the vicinity of the Cauvery shear zone, including a period of cooling in the kyanite stability field after an initial heating phase to ~725°C (at circa 535 Ma), followed by HP metamorphism during continental collision along the Cauvery shear zone, and finally slab delamination and UHT metamorphism at circa 525 Ma. Clearly, the prograde path experienced by the Northern Madurai Block rocks is very complex and often difficult to define, as early prograde assemblages in pelitic rocks are only very rarely preserved due to the high intensity of the peak HP-UHT metamorphism [*Clark et al*., 2014]. For this reason, we believe that the early prograde fabrics are poorly preserved throughout this region. The exhumation of the Northern Madurai Block following peak metamorphic conditions defined by steep NE-SW trending fabrics and subvertical mineral elongation lineations suggest a component of vertical extension during either horizontal NW-SE synconvergent shortening or diapiric upwelling of buoyant melt-dominated granitic crust during postorogenic collapse and extension. Steep decompression paths associated with rapid exhumation of up to 4 kbars [*Raith et al*., 1997; *Sajeev et al*., 2006; *Brandt et al*., 2011; *Clark et al*., 2014], a high angle between the plate boundary and displacement vector, as well as the short timing between peak metamorphism and decompression (~10–50 Ma) are all consistent with tectonic exhumation during continued ~N-S synconvergent thrusting in a dextral transpressive orogen [*Thompson et al*., 1997; *Dumond et al*., 2013]. In that regard, the KKPT shear zone (characterized by the steep fabrics and subvertical lineations) can be interpreted as representing a synconvergent thrust with footwall characterized by older, more rigid, crustal rocks to the west and the hanging wall by the younger, softer, metasedimentary rock units to the east. Continued decompression and cooling of the exhumed high-temperature lower crustal material at midcrustal levels most likely occurred during postcollisional collapse of an overthickened orogen (isobaric-cooling retrograde path of the existing and modeled P-T phase diagrams) [*Brown and Raith*, 1996; *Raith et al*., 1997; *Sajeev et al*., 2006; *Jamieson and Beaumont*, 2011]. This resulted in the formation of biotite through back reactions with the melt and growth of zircon at circa 518–512 Ma [*Clark et al*., 2014]. The predominant NE-SW to NNE-SSW (FN_2 and FN_3, respectively) trending folds and shape fabrics in the Northern Madurai Block along with the third generation folds (FK_3) of the PGT transect (here collectively grouped as D_3) are often accompanied by melt-induced shear bands, layer-parallel leucosomes, reclined folds, and subhorizontal to moderately plunging mineral elongations all suggesting deformation during vertical shortening and lateral extension. While shallow ~south plunging reclined folds with attenuated

lower limbs suggest south block-up movements during ~N-S shortening, care must be taken as complex fold patterns can arise due extensional tectonics during the collapse of an overthickened orogen [*Harris et al*., 2002]. The sinuous nature of the high-strain (Muthampatti-Palayam-Eriyody—MPE shear zone) and fold-dominated $D_{2/3}$ fabrics (from NE-SW trending in the north to NNE-SSW trending in the south) has been described as deformation due to an indenter located to the south-east of the Southern Granulite Terrane [*Cenki and Kriegsman*, 2005] or deformation during reverse thrusting of the "older" metasedimentary-dominated block onto the charnockite massifs west of the KKPT shear zone [*Srinivasan and Rajeshdurai*, 2010]. However, the interpretation of whether D_3 structures formed during shortening or extension is not straightforward. A number of observations support the argument for extensional deformation (D_3) during orogenic collapse. These include (1) an overprinting relationship of D_3 with the steep exhumation fabrics associated with D_2, (2) shallow to subhorizontal mineral elongation lineations suggesting lateral escape, and (3) the lack of evidence for increased pressures due to thrust thickening. In addition, *Harris et al*. [2002] demonstrated that folds can form parallel to trend of the shear zones as well as parallel to the transport direction if the detachment shear zone is undulating. Shallow-dipping muscovite-bearing gneissic foliations immediately south of the MPE shear zone provide evidence of lower metamorphic conditions, thus supporting the argument for extensional collapse. However, due to the lack of geochronological constraints and insufficient field observations, this interpretation warrants further investigation. The best estimate for the upper limit of D_3 deformation is provided by the 523–502 Ma ages of undeformed pegmatites (samples SI10-77 and SI10-112, this study). The latest deformational phase in the Northern Madurai Block (D_4) is associated with upper crustal deformation during bulk ~N-S shortening after 500 Ma.

A recently proposed model by *Brandt et al*. [2014], linking the post-Neoarchean Madurai Block evolution to that of the Eastern Ghats Orogen based on the U-Pb zircon geochronology, invokes up to ~200 km dextral offsets along the Cauvery shear zone. However, this is inconsistent with this study, which shows that the movement along the Cauvery shear zone is largely dip slip, with a minor component of strike-slip motion, rendering ~200 km dextral offsets unlikely. This is not even taking into account that no evidence of the widespread ~1.6 Ga metamorphism of the southern Eastern Ghats Orogen (otherwise known as the Krishna Orogen) [*Henderson et al*., 2014] is known from the Southern Granulite Terrane. Furthermore, *Brandt et al*.'s [2014] proposition of an early Paleoproterozoic granulite-facies metamorphism within the Northern Madurai Block based on SHRIMP U-Pb zircon dating of migmatitic grt-opx gneiss directly south (and possibly within) the Cauvery shear zone (their sample I-206-1-07) is unwarranted as the emplacement age of their magmatic protolith (2493 ± 10 Ma) is within error of their proposed granulite-facies metamorphic age of (2472 ± 15 Ma) and cannot, therefore, be separated into two distinct events. However, the 736 ± 55 Ma lower intercept in the same sample is within the proposed time scale for the deformation (D_3–D_4) associated with the high-strain fabrics within the Cauvery shear zone. In addition, the structural styles across the Cauvery shear zone (from Salem Block in the north to Madurai Block in the south) change significantly in character (Table 3) and timing, with much younger circa 550–500 Ma deformation characterizing the deformation in the Madurai Block when compared to the Cauvery shear zone and the Salem Block (Figure 11), further supporting the argument of a presence of major suture zone (i.e., Cauvery shear zone) between the two tectonic blocks. The link between metamorphism and deformation with the surrounding Gondwanan terranes of Madagascar and Sri Lanka is strengthened by this study. In the Antananarivo Block of central and eastern Madagascar, Neoarchean to Cryogenian charnockitic gneisses show early high-grade metamorphism at circa 550 Ma followed by retrogression to biotite-bearing assemblages and undeformed granitic dykes of circa 517 Ma, thus providing constraints for high-grade metamorphism and deformation [*Kröner et al*., 2000; *Collins et al*., 2001; *Raharimahefa and Kusky*, 2010]. This is in strong agreement with the timing of high-grade metamorphism and deformation (circa 550–510 Ma) obtained in this study. Similar late Neoproterozoic (circa 550–520 Ma) HP-UHT metamorphic conditions and complex decompression paths including an early isothermal decompression suggesting rapid exhumation of rocks comparable to those of the NMB have been reported from the Highland Complex of Sri Lanka as well as from the Lützow-Holm Bay of East Antarctica [*Fraser et al*., 2000; *Sajeev et al*., 2007]. From the Southern Granulite Terrane perspective, the evolution of the eastern margin of the East African Orogen during the late Neoproterozoic (circa 550–500 Ma) is interpreted as being characterized by significant thickening during continent-continent collision associated with dextral transpression

followed by rapid exhumation during postorogenic collapse. In this scenario, the Cauvery shear zone has played a pivotal role in bringing together the Indian and Madagascan blocks (the latter named Azania by *Collins and Pisarevsky* [2005]), during the closure of the Mozambique Ocean in the final stages of Gondwana formation.

6. Conclusions

The structural and temporal evolution of the Southern Granulite Terrane as determined from close field observations, satellite imagery, and U-Pb zircon geochronology has helped unravel the tectonic events that shaped this Proterozoic mobile belt. The results of this study show that the Palghat-Cauvery Shear System of anastomosing shear zones reflects a polydeformational history, with early Paleoproterozoic HP-HT granulite-facies metamorphism affecting the northern margins of the system, while the southern margins of the zone are shaped by Neoproterozoic magmatism and HP-UHT metamorphism. The study of the structural fabrics north and south of the Cauvery shear zone (the southern margin of the Palghat-Cauvery Shear System) shows that the late Neoproterozoic deformation was associated with dextral transpression. Finally, the timing of the HP-UHT metamorphism in the Cauvery shear zone and the Northern Madurai Block is constrained to 550–500 Ma.

Acknowledgments

This paper forms TRaX Record #321. The work presented here was funded by Australia-India Strategic Research Fund (AISRF) project ST030046, Australian Research Council grants FT120100340, DP0879330, and DE120103067, and an Australian Postgraduate Award to the senior author. We thank the two anonymous reviewers, who have significantly improved the manuscript. Chetty and Bhaskar Rao are thanked for assisting with logistics, discussions on the geology, and overall support throughout our field campaigns. Santosh is thanked for his constant collaboration and support on the geological evolution of the region and for introducing us to the area in the first place.

References

Anderson, J. R., J. L. Payne, D. E. Kelsey, M. Hand, A. S. Collins, and M. Santosh (2012), High-pressure granulites at the dawn of the Proterozoic, *Geology*, *40*(5), 431–434.

Appel, P., A. Möller, and V. Schenk (1998), High-pressure granulite facies metamorphism in the Pan-African belt of eastern Tanzania: P-T-t evidence against granulite formation by continent collision, *J. Metamorph. Geol.*, *16*(4), 491–509.

Bartlett, J. M., J. S. Dougherty-Page, N. B. W. Harris, C. J. Hawkesworth, and M. Santosh (1998), The application of single zircon evaporation and model Nd ages to the interpretation of polymetamorphic terrains: An example from the Proterozoic mobile belt of south India, *Contrib. Mineral. Petrol.*, *131*(2), 181–195.

Bhaskar Rao, Y. J., T. R. K. Chetty, A. S. Janardhan, and K. Gopalan (1996), Sm-Nd and Rb-Sr ages and P-T history of the Archean Sittampundi and Bhavani layered meta-anorthosite complexes in Cauvery shear zone, South India: Evidence for Neoproterozoic reworking of Archean crust, *Contrib. Mineral. Petrol.*, *125*(2), 237–250.

Bhaskar Rao, Y. J., A. S. Janardhan, T. Vijaya Kumar, B. L. Narayana, A. M. Dayal, P. N. Taylor, and T. R. K. Chetty (2003), Sm-Nd model ages and Rb-Sr isotope systematics of charnockites and gneisses across the Cauvery shear zone, southern India: Implications for the Archaean-Neoproterozoic boundary in the southern granulite terrain, in *Tectonics of Southern Granulite Terrain*, edited by M. Ranmakrishnan, *Geol. Soc. India Mem.*, *50*, 297–317.

Bhattacharya, S., M. Santosh, Z. Zhang, H. Huang, A. Banerjee, P. M. George, and K. Sajeev (2014), Imprints of Archean to Neoproterozoic crustal processes in the Madurai Block, Southern India, *J. Asian Earth Sci.*, *88*, 1–10.

Bhutani, R., S. Balakrishnan, C. Nevin, and S. Jeyabal (2007), Sm-Nd isochron ages from Southern Granulite Terrain, South India: Age of protolith and metamorphism, *Geochim. Cosmochim. Acta*, *71*(15), A89–A89.

Boger, S. D., and J. M. Miller (2004), Terminal suturing of Gondwana and the onset of the Ross-Delamerian Orogeny: The cause and effect of an early Cambrian reconfiguration of plate motions, *Earth Planet. Sci. Lett.*, *219*, 35–48.

Brandt, S., V. Schenk, M. M. Raith, P. Appel, A. Gerdes, and C. Srikantappa (2011), Late Neoproterozoic P-T evolution of HP-UHT granulites from the Palni Hills (South India): New constraints from phase diagram modelling, LA-ICP-MS zircon dating and in-situ EMP monazite dating, *J. Petrol.*, *52*(9), 1813–1856.

Brandt, S., M. M. Raith, V. Schenk, P. Sengupta, C. Srikantappa, and A. Gerdes (2014), Crustal evolution of the Southern Granulite Terrane, South India: New geochronological and geochemical data for felsic orthogneisses and granites, *Precambrian Res.*, *246*, 91–122.

Brown, M., and M. Raith (1996), First evidence of ultrahigh-temperature decompression from the granulite province of southern India, *J. Geol. Soc.*, *153*(6), 819–822.

Cawood, P. A., and C. Buchan (2007), Linking accretionary orogenesis with supercontinent assembly, *Earth Sci. Rev.*, *82*(3–4), 217–256.

Cenki, B., and L. M. Kriegsman (2005), Tectonics of the Neoproterozoic Southern Granulite Terrain, South India, *Precambrian Res.*, *138*(1–2), 37–56.

Cenki, B., I. Braun, and M. Bröcker (2004), Evolution of the continental crust in the Kerala Khondalite Belt, southernmost India: Evidence from Nd isotope mapping, U-Pb and Rb-Sr geochronology, *Precambrian Res.*, *134*(3–4), 275–292.

Chetty, T. R. K., and Y. J. Bhaskar Rao (2006a), Strain pattern and deformational history in the eastern part of the Cauvery shear zone, southern India, *J. Asian Earth Sci.*, *28*, 46–54.

Chetty, T. R. K., and Y. J. Bhaskar Rao (2006b), The Cauvery shear zone, Southern Granulite Terrain, India: A crustal-scale flower structure, *Gondwana Res.*, *10*(1–2), 77–85.

Chetty, T. R. K., and Y. J. Bhaskar Rao (2006c), Constrictive deformation in transpressional regime: Field evidence from the Cauvery shear zone, Southern Granulite Terrain, India, *J. Struct. Geol.*, *28*(4), 713–720.

Clark, C., A. S. Collins, M. Santosh, R. Taylor, and B. P. Wade (2009a), The P-T-t architecture of a Gondwanan suture: REE, U-Pb and Ti-in-zircon thermometric constraints from the Palghat Cauvery shear system, South India, *Precambrian Res.*, *174*(1–2), 129–144.

Clark, C., A. S. Collins, N. E. Timms, P. D. Kinny, T. R. K. Chetty, and M. Santosh (2009b), SHRIMP U-Pb age constraints on magmatism and high-grade metamorphism in the Salem Block, southern India, *Gondwana Res.*, *16*(1), 27–36.

Clark, C., D. Healy, T. Johnson, A. S. Collins, R. J. Taylor, M. Santosh, and N. E. Timms (2014), Hot orogens and supercontinent amalgamation: A Gondwanan example from southern India, *Gondwana Res.*, doi:10.1016/j.gr.2014.11.005.

Collins, A., B. Windley, A. Kröner, I. Fitzsimons, and B. Hulscher (2001), The tectonic architecture of central Madagascar: Implication on the evolution of the East African Orogeny, *Gondwana Res.*, *4*(2), 152–153.

Collins, A. S. (2006), Madagascar and the amalgamation of Central Gondwana, *Gondwana Res.*, *9*, 3–16.

Collins, A. S., and S. A. Pisarevsky (2005), Amalgamating eastern Gondwana: The evolution of the Circum-Indian Orogens, *Earth Sci. Rev.*, *71*(3–4), 229–270.
Collins, A. S., and B. F. Windley (2002), The tectonic evolution of central and northern Madagascar and its place in the final assembly of Gondwana, *J. Geol.*, *110*(3), 325.
Collins, A. S., A. Kröner, I. C. W. Fitzsimons, and T. Razakamanana (2003), Detrital footprint of the Mozambique Ocean: U-Pb SHRIMP and Pb evaporation zircon geochronology of metasedimentary gneisses in eastern Madagascar, *Tectonophysics*, *375*(1–4), 77–99.
Collins, A. S., C. Clark, K. Sajeev, M. Santosh, D. E. Kelsey, and M. Hand (2007a), Passage through India: The Mozambique Ocean suture, high-pressure granulites and the Palghat-Cauvery shear zone system, *Terra Nova*, *19*(2), 141–147.
Collins, A. S., M. Santosh, I. Braun, and C. Clark (2007b), Age and sedimentary provenance of the southern granulites, South India: U-Th-Pb SHRIMP secondary ion mass spectrometry, *Precambrian Res.*, *155*, 125–138.
Collins, A. S., et al. (2014a), Detrital mineral age, radiogenic isotopic stratigraphy and tectonic significance of the Cuddapah Basin, India, *Gondwana Res.*, doi:10.1016/j.gr.2014.10.013.
Collins, A. S., C. Clark, and D. Plavsa (2014b), Peninsular India in Gondwana: The tectonothermal evolution of the Southern Granulite Terrain and its Gondwanan counterparts, *Gondwana Res.*, *25*(1), 190–203.
Corfu, F., J. M. Hanchar, P. W. O. Hoskin, and P. Kinny (2003), Atlas of zircon textures, *Rev. Mineral. Geochem.*, *53*(1), 469–500.
Drury, S. A., and R. W. Holt (1980), The tectonic framework of the South Indian craton: A reconnaissance involving LANDSAT imagery, *Tectonophysics*, *65*(3–4), T1–T15.
Drury, S. A., N. B. W. Harris, R. W. Holt, G. J. Reeves-Smith, and R. T. Wightman (1984), Precambrian tectonics and crustal evolution in South India, *J. Geol.*, *92*(1), 3–20.
Dumond, G., K. H. Mahan, M. L. Williams, and M. J. Jercinovic (2013), Transpressive uplift and exhumation of continental lower crust revealed by synkinematic monazite reactions, *Lithosphere*, *5*(5), 507–512.
Fraser, G., I. McDougall, D. J. Ellis, and I. S. Williams (2000), Timing and rate of isothermal decompression in Pan-African granulites from Rundvågshetta, East Antarctica, *J. Metamorph. Geol.*, *18*(4), 441–454.
Fritz, H., et al. (2013), Orogen styles in the East African Orogen: A review of the Neoproterozoic to Cambrian tectonic evolution, *J. Afr. Earth Sci.*, *86*, 65–106.
Ghosh, J. G., M. J. D. Wit, and R. E. Zartman (2004), Age and tectonic evolution of Neoproterozoic ductile shear zones in the Southern Granulite Terrain of India, with implications for Gondwana studies, *Tectonics*, *23*(3), 1–38, doi:10.1029/2002TC001444.
Glorie, S., J. De Grave, T. Singh, J. L. Payne, and A. S. Collins (2014), Crustal root of the Eastern Dharwar Craton: Zircon 1 U-Pb age and Lu-Hf isotopic evolution of the East Salem Block, southeast India, *Precambrian Res.*, *249*, 229–246.
Hansen, E. C., and D. E. Harlov (2007), Whole-rock, phosphate, and silicate compositional trends across an amphibolite- to granulite-facies transition, Tamil Nadu, India, *J. Petrol.*, *48*(9), 1641–1680.
Harris, L. B., H. A. Koyi, and H. Fossen (2002), Mechanisms for folding of high-grade rocks in extensional tectonic settings, *Earth Sci. Rev.*, *59*(1–4), 163–210.
Henderson, B., A. S. Collins, J. Payne, C. Forbes, and D. Saha (2014), Geologically constraining India in Columbia: The age, isotopic provenance and geochemistry of the protoliths of the Ongole Domain, Southern Eastern Ghats, India, *Gondwana Res.*, *26*(3–4), 888–906.
Hoskin, P. W. O., and L. P. Black (2000), Metamorphic zircon formation by solid-state recrystallization of protolith igneous zircon, *J. Metamorph. Geol.*, *18*(4), 423–439.
Jackson, S. E., N. J. Pearson, W. L. Griffin, and E. A. Belousova (2004), The application of laser ablation-inductively coupled plasma-mass spectrometry to in situ U-Pb zircon geochronology, *Chem. Geol.*, *211*(1–2), 47–69.
Jacobs, J., and R. J. Thomas (2004), Himalayan-type indenter-escape tectonics model for the southern part of the late Neoproterozoic-Early Paleozoic East African-Antarctic orogen, *Geology*, *32*(8), 721–724.
Jamieson, R. A., and C. Beaumont (2011), Coeval thrusting and extension during lower crustal ductile flow—Implications for exhumation of high-grade metamorphic rocks, *J. Metamorph. Geol.*, *29*(1), 33–51.
Janardhan, A. S., R. C. Newton, and J. V. Smith (1979), Ancient crustal metamorphism at low pH2O: Charnockite formation at Kabbaldurga, South India, *Nature*, *278*(5704), 511–514.
Johnson, P. R., A. Andresen, A. S. Collins, A. R. Fowler, H. Fritz, W. Ghebreab, T. Kusky, and R. J. Stern (2011), Late Cryogenian-Ediacaran history of the Arabian-Nubian Shield: A review of depositional, plutonic, structural, and tectonic events in the closing stages of the northern East African Orogen, *J. Afr. Earth Sci.*, *61*(3), 167–232.
Johnson, T. E., C. Clark, R. J. Taylor, M. Santosh, and A. S. Collins (2015), Prograde and retrograde growth of monazite in migmatites: An example from the Nagercoil Block, southern India, *Geosci. Front.*, doi:10.1016/j.gsf.2014.12.003.
Jöns, N., and V. Schenk (2011), The ultrahigh temperature granulites of southern Madagascar in a polymetamorphic context: Implications for the amalgamation of the Gondwana supercontinent, *Eur. J. Mineral.*, *23*, 127–156.
Kelsey, D. E., C. Clark, and M. Hand (2008), Thermobarometric modelling of zircon and monazite growth in melt-bearing systems: Examples using model metapelitic and metapsammitic granulites, *J. Metamorph. Geol.*, *26*, 199–212.
Kooijman, E., D. Upadhyay, K. Mezger, M. M. Raith, J. Berndt, and C. Srikantappa (2011), Response of the U-Pb chronometer and trace elements in zircon to ultrahigh-temperature metamorphism: The Kadavur anorthosite complex, southern India, *Chem. Geol.*, *290*(3–4), 177–188.
Kriegsman, L. M. (1995), The Pan-African event in East Antarctica: A view from Sri Lanka and the Mozambique Belt, *Precambrian Res.*, *75*(3–4), 263–277.
Kröner, A., E. Hegner, A. S. Collins, B. F. Windley, T. S. Brewer, T. Razakamanana, and R. T. Pidgeon (2000), Age and magmatic history of the Antanarivo Block, Central Madagascar, as derived from zircon geochronology and Nd isotopic systematics, *Am. J. Sci.*, *300*, 251–288.
Meert, J. G. (2003), A synopsis of events related to the assembly of eastern Gondwana, *Tectonophysics*, *362*(1–4), 1–40.
Meert, J. G., and R. Van Der Voo (1997), The assembly of Gondwana 800–550 Ma, *J. Geodyn.*, *23*(3–4), 223–235.
Meißner, B., P. Deters, C. Srikantappa, and H. Köhler (2002), Geochronological evolution of the Moyar, Bhavani and Palghat shear zones of southern India: Implications for east Gondwana correlations, *Precambrian Res.*, *114*(1–2), 149–175.
Mohan, M. R., M. Satyanarayanan, M. Santosh, P. J. Sylvester, M. Tubrett, and R. Lam (2013), Neoarchean suprasubduction zone arc magmatism in southern India: Geochemistry, zircon U-Pb geochronology and Hf isotopes of the Sittampundi Anorthosite Complex, *Gondwana Res.*, *23*(2), 539–557.
Muhongo, S., and J. L. Lenoir (1994), Pan-African granulite-facies metamorphism in the Mozambique Belt of Tanzania: U-Pb zircon geochronology, *J. Geol. Soc.*, *151*(2), 343–347.
Noack, N. M., R. Kleinschrodt, M. Kirchenbaur, R. O. C. Fonseca, and C. Münker (2013), Lu-Hf isotope evidence for Paleoproterozoic metamorphism and deformation of Archean oceanic crust along the Dharwar Craton margin, southern India, *Precambrian Res.*, *233*, 206–222.
Peucat, J.-J., M. Jayananda, D. Chardon, R. Capdevila, C. M. Fanning, and J.-L. Paquette (2013), The lower crust of the Dharwar Craton, Southern India: Patchwork of Archean granulitic domains, *Precambrian Res.*, *227*, 4–28.
Pichamuthu, C. S. (1960), Charnockite in the making, *Nature*, *188*(4745), 135–136.

Plavsa, D., A. S. Collins, J. F. Foden, L. Kropinski, M. Santosh, T. R. K. Chetty, and C. Clark (2012), Delineating crustal domains in Peninsular India: Age and chemistry of orthopyroxene-bearing felsic gneisses in the Madurai Block, *Precambrian Res.*, *198–199*, 77–93.
Plavsa, D., A. S. Collins, J. L. Payne, J. D. Foden, C. Clark, and M. Santosh (2014), Detrital zircons in basement metasedimentary protoliths unveil the origins of southern India, *Geol. Soc. Am. Bull.*, *126*(5–6), 791–811.
Prakash, D., M. Arima, and A. Mohan (2006), Ultrahigh-temperature metamorphism in the Palni Hills, South India: Insights from feldspar thermometry and phase equilibria, *Int. Geol. Rev.*, *48*(7), 619–638.
Prakash, D., S. Prakash, and H. K. Sachan (2010), Petrological evolution of the high pressure and ultrahigh-temperature mafic granulites from Karur, southern India: Evidence for decompressive and cooling retrograde trajectories, *Mineral. Petrol.*, *100*(1–2), 35–53.
Raharimahefa, T., and T. M. Kusky (2010), Temporal evolution of the Angavo and related shear zones in Gondwana: Constraints from LA-MC-ICP-MS U-Pb zircon ages of granitoids and gneiss from central Madagascar, *Precambrian Res.*, *182*(1–2), 30–42.
Raith, M., S. Karmakar, and M. Brown (1997), Ultra-high-temperature metamorphism and multistage decompressional evolution of sapphirine granulites from the Palni Hill Ranges, southern India, *J. Metamorph. Geol.*, *15*(3), 379–399.
Raith, M. M., C. Srikantappa, D. Buhl, and H. Koehler (1999), The Nilgiri enderbites, South India: Nature and age constraints on protolith formation, high-grade metamorphism and cooling history, *Precambrian Res.*, *98*(1–2), 129–150.
Raith, M. M., P. Sengupta, E. Kooijman, D. Upadhyay, and C. Srikantappa (2010), Corundum-leucosome-bearing aluminous gneiss from Ayyarmalai, Southern Granulite Terrain, India: A textbook example of vapor phase-absent muscovite-melting in silica-undersaturated aluminous rocks, *Am. Mineral.*, *95*(7), 897–907.
Ramakrishnan, M. (1993), Tectonic evolution of granulite terrains of southern India, in *Continental Crust of South India*, edited by B. P. Radhakrishna, *Geol. Surv. India Mem.*, *25*, 35–44.
Rao, T. V. S., B. L. Narayana, and K. Gopalan (1994), Rb-Sr age of the Sivamalai alkaline complex, Tamil Nadu, *Proc. Indian Acad. Sci. (Earth Planet Sci.)*, *103*(3), 425–437.
Reddy, S. M., A. S. Collins, C. Buchan, and A. H. Mruma (2004), Heterogeneous excess argon and Neoproterozoic heating in the Usagaran Orogen, Tanzania, revealed by single grain 40Ar/39Ar thermochronology, *J. Afr. Earth Sci.*, *39*(3–5), 165–176.
Robinson, F. A., J. D. Foden, A. S. Collins, and J. L. Payne (2014), Arabian Shield magmatic cycles and their relationship with Gondwana assembly: Insights from zircon U-Pb and Hf isotopes, *Earth Planet. Sci. Lett.*, *408*, 207–225.
Rubatto, D., I. S. Williams, and I. S. Buick (2001), Zircon and monazite response to prograde metamorphism in the Reynolds Range, central Australia, *Contrib. Mineral. Petrol.*, *140*(4), 458–468.
Saitoh, Y., T. Tsunogae, M. Santosh, T. R. K. Chetty, and K. Horie (2011), Neoarchean high-pressure metamorphism from the northern margin of the Palghat-Cauvery Suture Zone, southern India: Petrology and zircon SHRIMP geochronology, *J. Asian Earth Sci.*, *42*(3), 268–285.
Sajeev, K., Y. Osanai, and M. Santosh (2004), Ultrahigh-temperature metamorphism followed by two-stage decompression of garnet–orthopyroxene-sillimanite granulites from Ganguvarpatti, Madurai block, southern India, *Contrib. Mineral. Petrol.*, *148*(1), 29–46.
Sajeev, K., M. Santosh, and H. S. Kim (2006), Partial melting and P-T evolution of the Kodaikanal Metapelite Belt, southern India, *Lithos*, *92*(3–4), 465–483.
Sajeev, K., Y. Osanai, J. A. D. Connolly, S. Suzuki, J. Ishioka, H. Kagami, and S. Rino (2007), Extreme crustal metamorphism during a Neoproterozoic event in Sri Lanka: A study of dry mafic granulites, *J. Geol.*, *115*(5), 563–582.
Santosh, M. (1996), The Trivandrum and Nagercoil granulite blocks, *Gondwana Res. Group Mem.*, *3*, 243–277.
Santosh, M., N. B. W. Harris, D. H. Jackson, and D. P. Mattey (1990), Dehydration and Incipient Charnockite Formation: A phase equilibria and fluid inclusion study from South India, *J. Geol.*, *98*(6), 915–926.
Santosh, M., K. Yokoyama, S. Biju-Sekhar, and J. J. W. Rogers (2003), Multiple tectonothermal events in the granulite blocks of southern India revealed from EPMA dating: Implications on the history of supercontinents, *Gondwana Res.*, *6*(1), 29–63.
Santosh, M., A. S. Collins, I. Tamashiro, S. Koshimoto, Y. Tsutsumi, and K. Yokoyama (2006), The timing of ultrahigh-temperature metamorphism in southern India: U-Th-Pb electron microprobe ages from zircon and monazite in sapphirine-bearing granulites, *Gondwana Res.*, *10*(1–2), 128–155.
Santosh, M., S. Maruyama, and K. Sato (2009), Anatomy of a Cambrian suture in Gondwana: Pacific-type orogeny in southern India?, *Gondwana Res.*, *16*(2), 321–341.
Santosh, M., W. J. Xiao, T. Tsunogae, T. R. K. Chetty, and T. Yellappa (2012), The Neoproterozoic subduction complex in southern India: SIMS zircon U-Pb ages and implications for Gondwana assembly, *Precambrian Res.*, *192–195*, 190–208.
Santosh, M., Q.-Y. Yang, E. Shaji, T. Tsunogae, M. R. Mohan, and M. Satyanarayanan (2015), An exotic Mesoarchean microcontinent: The Coorg Block, southern India, *Gondwana Res.*, *27*(1), 165–195.
Sato, K., M. Santosh, T. Tsunogae, T. R. K. Chetty, and T. Hirata (2011a), Subduction-accretion-collision history along the Gondwana suture in southern India: A laser ablation ICP-MS study of zircon chronology, *J. Asian Earth Sci.*, *40*(1), 162–171.
Sato, K., M. Santosh, T. Tsunogae, T. R. K. Chetty, and T. Hirata (2011b), Laser ablation ICP mass spectrometry for zircon U-Pb geochronology of metamorphosed granite from the Salem Block: Implication for Neoarchean crustal evolution in southern India, *J. Mineral. Petrol. Sci.*, *106*(1), 1–12.
Sláma, J., et al. (2008), Plešovice zircon—A new natural reference material for U-Pb and Hf isotopic microanalysis, *Chem. Geol.*, *249*(1–2), 1–35.
Sommer, H., A. Kröner, S. Muhongo, and C. Hauzenberger (2005), SHRIMP zircon ages for post-Usagaran granitoid and rhyolitic rocks from the Palaeoproterozoic terrain of southwestern Tanzania, *S. Afr. J. Geol.*, *108*(2), 247–256.
Srinivasan, V., and P. Rajeshdurai (2010), The Suruli shear zone and regional scale folding pattern in Madurai Block of Southern Granulite Terrain, South India, *J. Earth Syst. Sci.*, *119*(2), 147–160.
Stern, R. J. (2002), Crustal evolution in the East African Orogen: A neodymium isotopic perspective, *J. Afr. Earth Sci.*, *34*(3–4), 109–117.
Teale, W., A. S. Collins, J. Foden, J. L. Payne, D. Plavsa, T. R. K. Chetty, M. Santosh, and M. Fanning (2011), Cryogenian (~830 Ma) mafic magmatism and metamorphism in the Northern Madurai Block, southern India: A magmatic link between Sri Lanka and Madagascar?, *J. Asian Earth Sci.*, *42*(3), 223–233.
Thompson, A. B., K. Schulmann, and J. Jezek (1997), Thermal evolution and exhumation in obliquely convergent (transpressive) orogens, *Tectonophysics*, *280*(1–2), 171–184.
Tomson, J. K., Y. J. Bhaskar Rao, T. Vijaya Kumar, and J. Mallikharjuna Rao (2006), Charnockite genesis across the Archaean-Proterozoic terrane boundary in the South Indian Granulite Terrain: Constraints from major-trace element geochemistry and Sr-Nd isotopic systematics, *Gondwana Res.*, *10*(1–2), 115–127.
Tomson, J. K., Y. J. Bhaskar Rao, T. Vijaya Kumar, and A. K. Choudhary (2013), Geochemistry and neodymium model ages of Precambrian charnockites, Southern Granulite Terrain, India: Constraints on terrain assembly, *Precambrian Res.*, *227*, 295–315.
Tsunogae, T., D. J. Dunkley, K. Horie, T. Endo, T. Miyamoto, and M. Kato (2014), Petrology and SHRIMP zircon geochronology of granulites from Vesleknausen, Lützow-Holm Complex, East Antarctica: Neoarchean magmatism and Neoproterozoic high-grade metamorphism, *Geosci. Front.*, *5*(2), 167–182.

Tucker, R. D., J. Y. Roig, C. Delor, Y. Amelin, P. Goncalves, M. H. Rabarimanana, A. V. Ralison, and R. W. Belcher (2011a), Neoproterozoic extension in the Greater Dharwar Craton: A reevaluation of the Betsimisaraka suture in Madagascar, *Can. J. Earth Sci.*, *48*(2), 389–417.

Tucker, R. D., J. Y. Roig, P. H. Macey, C. Delor, Y. Amelin, R. A. Armstrong, M. H. Rabarimanana, and A. V. Ralison (2011b), A new geological framework for south-central Madagascar; and its relevance to the "out-of-Africa" hypothesis, *Precambrian Res.*, *185*, 109–130.

Vavra, G., D. Gebauer, R. Schmid, and W. Compston (1996), Multiple zircon growth and recrystallization during polyphase Late Carboniferous to Triassic metamorphism in granulites of the Ivrea Zone (Southern Alps): An ion microprobe (SHRIMP) study, *Contrib. Mineral. Petrol.*, *122*(4), 337–358.

Yellappa, T., T. R. K. Chetty, T. Tsunogae, and M. Santosh (2010), The Manamedu Complex: Geochemical constraints on Neoproterozoic suprasubduction zone ophiolite formation within the Gondwana suture in southern India, *J. Geodyn.*, *50*(3–4), 268–285.

Yellappa, T., M. Santosh, T. R. K. Chetty, S. Kwon, C. Park, P. Nagesh, D. P. Mohanty, and V. Venkatasivappa (2012), A Neoarchean dismembered ophiolite complex from southern India: Geochemical and geochronological constraints on its suprasubduction origin, *Gondwana Res.*, *21*(1), 246–265.